Quaternary Science Reviews 290 (2022) 107620

Contents lists available at ScienceDirect

Quaternary Science Reviews

journal homepage: www.elsevier.com/locate/quascirev

Lacustrine diatom oxygen isotopes as palaeo precipitation proxy - Holocene environmental and snowmelt variations recorded at Lake Bolshoye Shchuchye, Polar Urals, Russia

Hanno Meyer [a, *], Svetlana S. Kostrova [a], Philip Meister [a], Marlene M. Lenz [b], Gerhard Kuhn [c], Larisa Nazarova [a], Liudmila S. Syrykh [d], Yury Dvornikov [e]

[a] Alfred Wegener Institute Helmholtz Centre for Polar and Marine Research, Research Unit Potsdam, Telegrafenberg A45, Potsdam 14473, Germany
[b] Institute of Geology and Mineralogy, University of Cologne, Zülpicher Str. 49a, Cologne 50674, Germany
[c] Alfred Wegener Institute Helmholtz Centre for Polar and Marine Research, Am Alten Hafen 26, Bremerhaven 27568, Germany
[d] Herzen State Pedagogical University of Russia, Moika 48, St. Petersburg 191186, Russia
[e] Department of Landscape Design and Sustainable Ecosystems, Agrarian-Technological Institute, Peoples' Friendship University of Russia (RUDN University), 6 Miklukho-Maklaya St, Moscow, 117198, Russia

ARTICLE INFO

Article history:
Received 28 January 2022
Received in revised form
20 June 2022
Accepted 21 June 2022
Available online 12 July 2022

Handling Editor: P Rioual

Keywords:
Stable oxygen isotopes
Hydrological fluctuations
Biogenic silica
Diatoms
Climate change
Chironomids
Lake sediments

ABSTRACT

The diatom oxygen isotope composition ($\delta^{18}O_{diatom}$) from lacustrine sediments helps tracing the hydrological and climate dynamics in individual lake catchments, and is generally linked to changes in temperature and $\delta^{18}O_{lake}$. Lake Bolshoye Shchuchye (67°53′N; 66°19′ E; 186 m a.s.l) is the largest and deepest freshwater reservoir in the Polar Urals, Arctic Russia. The diatom oxygen isotope interpretation is supported by modern (isotope) hydrology, local bioindicators such as chironomids, isotope mass-balance modelling and a digital elevation model of the catchment.

The Bolshoye Shchuchye $\delta^{18}O_{diatom}$ record generally follows a decrease in summer insolation and the northern hemisphere (NH) temperature history. However, it displays exceptional, short-term variations exceeding 5‰, especially in Mid and Late Holocene. This centennial-scale variability occurs roughly contemporaneously with and similar in frequency to Holocene NH glacier advances. However, larger Holocene glacier advances in the Lake Bolshoye Shchuchye catchment are unknown and have not left any significant imprint on the lake sediment record. As Lake Bolshoye Shchuchye is deep and voluminous, about 30–50% of its volume needs to be exchanged with isotopically different water within decades to account for these shifts in the $\delta^{18}O_{diatom}$ record. A plausible source of water with light isotope composition inflow is snow, known to be transported in surplus by snow redistribution from the windward to the leeward side of the Polar Urals. Here, we propose snow melt variability and associated influx changes being the dominant mechanism responsible for the observed short-term changes in the $\delta^{18}O_{diatom}$ record. This is the first time such drastic, centennial-scale hydrological changes in a catchment have been identified in Holocene lacustrine diatom oxygen isotopes, which, for Lake Bolshoye Shchuchye, are interpreted as proxy for palaeo precipitation and, on millennial timescales, for summer temperatures.

1. Introduction

The ongoing climate warming is currently being debated at scientific, political and social levels. Comparisons with past climatic conditions are generally used to assess the stability or instability of regional environments as well as the potential to predict possible trends of future climate change. This is important for policymakers today and for human well-being in the future as food and water supply, energy production and use largely depend on the successful reconstructions of climatic conditions that existed in the past (IPCC, 2014; NOAA NCEI, 2020).

Glaciers and ice or snow fields are visual indicators for climate changes in high mountain regions (Davis et al., 2009; Khromova et al., 2014, 2019; Solomina et al., 2015; WGMS, 2017). Their advances and retreats do not only significantly alter landscapes (Khromova et al., 2019), but can also increase risks of local hazards

* Corresponding author.
E-mail address: hanno.meyer@awi.de (H. Meyer).

https://doi.org/10.1016/j.quascirev.2022.107620

and natural disasters (Huggel et al., 2008; Petrakov et al., 2008; Khromova et al., 2019). Changes in glacier mass balances lead to rearrangements of local and regional water cycles (Koboltschnig and Schöner, 2011; Radić and Hock, 2014; Nazarova et al., 2021a) and may be linked to global sea level rise (Shahgedanova et al., 2012; Gardner et al., 2013).

The Ural Mountains are a north-to-south stretching range of more than 2000 km, separating Europe and Asia. As such, it is an orographic barrier playing an important role for atmospheric moisture transport to the Eurasian Arctic (i.e. Svendsen et al., 2004). In this region, small glaciers are widespread, mainly in the Polar Urals (Kononov et al., 2005; Shahgedanova et al., 2012; Khromova et al., 2014; Solomina et al., 2015; Svendsen et al., 2019). Field-based and satellite observations revealed that significant changes in air temperature and precipitation in recent decades have caused a reduction of the glacier areas in the Polar Urals by 23% on average (Nosenko and Tsvetkov, 2003; Shahgedanova et al., 2012; Khromova et al., 2014, 2019). Although numerous studies have contributed to a better understanding of the climate and environmental history in the Polar Urals (Panova et al., 2003; Cremer et al., 2004; Andreev et al., 2005; Jankovská et al., 2006; Solovieva et al., 2008; Regnéll et al., 2019; Nazarova et al., 2021b), the glacier fluctuations in this region are still very poorly investigated (Kononov et al., 2005; Solomina et al., 2010, 2015; Haflidason et al., 2019) and existing knowledge of the glacier dynamics history remains fragmentary (Mangerud et al., 2008; Astakhov, 2018; Svendsen et al., 2014, 2019).

Continuous reconstructions of glacier size variations are based on information provided by different parameters from lake sediments, e.g. magnetic susceptibility, loss-on-ignition, grain-size variations, and chemical element contents (Dahl et al., 2003; Nesje, 2009; Nesje et al., 2014; Regnéll et al., 2019; Lenz et al., 2021). The oxygen isotope composition of diatoms ($\delta^{18}O_{diatom}$) has been widely used as a proxy for climate and hydrological changes in many studies (Swann and Leng, 2009; van Hardenbroek et al., 2018). Shifts in diatom oxygen isotope records (Kostrova et al., 2013, 2019, 2021; Meyer et al., 2015; Cartier et al., 2019), often reflect changes in lake water ($\delta^{18}O_{lake}$) related to variations in atmospheric precipitation patterns and/or in the hydrological conditions in the catchment. Generally, evaporative and inflow processes (i.e. by glacial meltwaters) have been identified as key processes within lakes. $\delta^{18}O_{diatom}$, consequently, has a high potential to enhance our understanding of coupled glacier-lake dynamics beyond instrumental records.

In the current study, $\delta^{18}O_{diatom}$ from Lake Bolshoye Shchuchye (Fig. 1) has been employed as novel proxy to trace environmental and climatic fluctuations in the Polar Urals through the Holocene. Our approach is supported by lake-internal proxies (i.e. chironomid and biogeochemical analyses) of the same sedimentary succession, complemented by modern isotope hydrology and isotope mass-balance modelling. The newly obtained $\delta^{18}O_{diatom}$ record is discussed in the context of other regional and hemispheric environmental reconstructions (Shemesh et al., 2001; Andreev et al., 2005; Jankovská et al., 2006; Heikkilä et al., 2010; Regnéll et al., 2019; Svendsen et al., 2019; Kostrova et al., 2019; Lenz et al., 2021; Cowling et al., 2021) including glacier fluctuations in order to explore the response of the lake system to hydroclimate change.

2. Study area

Lake Bolshoye Shchuchye (67°53′N; 66°19′ E; 186 m a.s.l) is the largest and deepest freshwater reservoir of the Polar Urals, Arctic

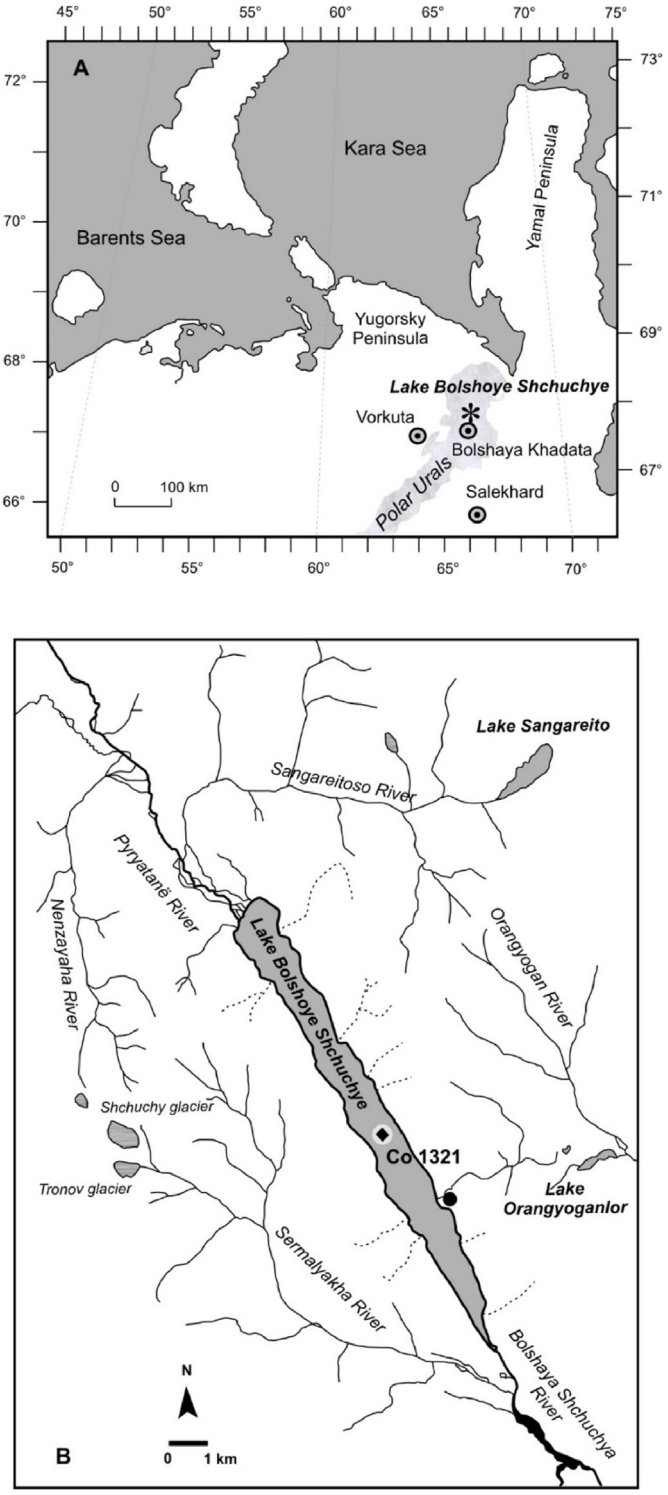

Fig. 1. (A) Schematic maps of the Polar Urals including the study site and other points of interest modified from Andreev et al. (2005). (B) Location of Lake Bolshoye Shchuchye (67°53′N; 66°19′ E; 186 m a.s.l.) with the position of the Co 1321 sediment core (black diamond) and the water sampling site (grey circle); as well as location of the snow cover column (black circle). The sketch was adapted from Regnéll et al. (2019). The Shchuchy and Tronov glaciers are outside the Lake Bolshoye Shchuchye catchment.

Russia, located in the permafrost zone at the boundary between Europe and Asia (Fig. 1). The lake surface area is 11.8 km^2, with mean and maximum water depths of 78.2 m and 160.0 m, respectively (Pechkin et al., 2017). The lake basin consists of a tectonic, glacially-eroded and overdeepened V-shaped mountain valley (Kemmerich, 1966; Svendsen et al., 2019; Haflidason et al., 2019) orientated northwest to southeast (Fig. 1B). With an average width of 0.92 km (maximum of 1.35 km) and a length of 12.7 km (Bogdanov et al., 2004), the lake is clearly elongated in shape. The lake is surrounded by ridges which peak up to more than 1000 m (Kemmerich, 1966). The lake basin is characterised by steep slopes and a sharp increase in depth in the central part and more gentle slopes in the northwestern and southeastern parts (Kemmerich, 1966; Pechkin et al., 2017). The bedrock comprises Proterozoic-Cambrian basaltic and andesitic rocks in the eastern and northwestern parts of the catchment and Ordovician quartzite and phyllitic rocks in the southwestern catchment (Dushin et al., 2009; Lammers et al., 2019; Svendsen et al., 2019). The catchment area of ~227 km^2 consists of a narrow zone along the lake as well as a wider hinterland to the north (Bogdanov et al., 2004). The lake is a hydrologically open system fed by 12 ephemeral streams with Pyryanatanë River as the main inflow forming a delta at the lake's northern end (Bogdanov et al., 2004). The Bolshaya Shchuchya River outflows at the southern part of the lake (Fig. 1B). The annual runoff from the catchment area is around 0.13–0.15 km^3 a^{-1} and about 5–7 years of residence time are required to renew the whole volume of water (~1 km^3) stored in the lake basin (Haflidason et al., 2019).

Lake Bolshoye Shchuchye is monomictic with mixing occurring only during the very short summer periods (Svendsen et al., 2019). The lake water temperature is persistently low, reaching 1.2–3.1 °C beneath the ice (Regnéll et al., 2019) and a mean surface water temperature not exceeding 10–14°C even on very hot days in August (Mitrofanova, 2017; Vinokurova, 2017). The lake is typically ice-covered for more than half a year, from early October to ice-out in late June–early July (Kemmerich, 1966; Svendsen et al., 2019). The lake ecosystem is pristine and not subject to anthropogenic impact and changes only under the influence of natural factors (Yermolaeva and Burmistrova, 2017).

The regional climate is continental and quite severe with long, cold winters and short, cool summers. The catchment is characterised by excessive moisture with a lack of heat (Morozova et al., 2006). The average annual air temperature is −6.3 °C (at the Bolshaya Khadata station (260 m a.s.l) located ~25 km to the south of Lake Bolshoye Shchuchye; Fig. 1A), ranging from −14.3 °C (winter) to +7.0 °C (summer) (Solomina et al., 2010). Annual precipitation amounts are around 610 mm with the sum of warm period precipitation of 70 mm on average (Solomina et al., 2010; Shahgedanova et al., 2012). There are a few cirque- and niche-type glaciers less than 1 km^2 in size near the lake catchment today (Solomina et al., 2010; Khromova et al., 2014; Regnéll et al., 2019). However, glaciers almost disappeared in response to the recent climate warming (Svendsen et al., 2019).

The hydroclimate in this region reflects the trajectories of prevailing air masses. Typically, westerly cyclones originating over the Northern Atlantic dominate in winter, bringing cloudy, windy weather and precipitation (Kemmerich, 1966; Kononov et al., 2005; Shahgedanova et al., 2012; Pischalnikova, 2016). These are also related to strong winds that cause snow redistribution within mountains and its accumulation on leeward slopes and depressions (Mangerud et al., 2008). In summer, dry continental air masses from the east provide conditions for relatively hot and dry weather, whereas incursions of northwesterly and northerly cyclones often cause rain and a sharp drop in air temperatures (Kemmerich, 1966; Kononov et al., 2005).

3. Materials and methods

3.1. Sediment recovery, core lithology and chronology

In April 2016, a 54-m-long sediment core (Co 1321; 67°53′ N, 66°19′ E; water depth: 136 m) was retrieved from the central part of Lake Bolshoye Shchuchye using gravity and percussion piston corers (UWITEC Ltd., Austria) from the central part of Lake Bolshoye Shchuchye (Fig. 1). The depth interval from 9.15 to 0 mcd (meter composite depth) of the core, consisting of grey to brown fine-grained, diffusely layered, hemipelagic sediment intermitted by turbidite layers, is the focus of this paper. A recent study (Lenz et al., 2021) demonstrated that the upper 9.15-m part was deposited during the last ~11,400 years (calibrated ages are used consistently in this study), i.e. covers the Holocene interglacial. The age-depth relationship of the analysed part of the Co1321 core is based on the surface age (2016 CE; Common Era) and five AMS ^{14}C dates. Details for the Holocene part of the age model are summarised in the supplement (Fig. S1 and Table S1; based on Lenz et al., 2021). Uncalibrated ^{14}C ages have individual error bars between ±18 and ± 57 years (Lenz et al., 2021). The age model was calculated with CLAM version 2.3.9 (Blaauw, 2010, 2021), which was run in R version 4.0.3 (R Core Team, 2020). The Holocene onset at ~11.5 cal Ka BP is supported by the results of pollen analysis with a notable increase in tree pollen together with a decrease in herb pollen (Lenz et al., 2021). A detailed description of the age model and lake internal parameters of Lake Bolshoye Shchuchye also beyond the Holocene part of core Co1321are given in Lenz et al. (2021).

3.2. Geochemical analyses

The Co 1321 core was X-ray fluorescence (XRF)-scanned at 1-mm resolution using an ITRAX core scanner (Cox Analytical, Sweden) at the University of Cologne. Sub-sampling for total carbon (TC) and total inorganic carbon (TIC) analyses was done at 8-cm intervals omitting turbidites, which offers a temporal resolution of about 100 years between two samples. TC and TIC contents were measured with a DIMATOC 2000 carbon analyser (Dimatec Corp., Germany). Total organic carbon (TOC) was calculated by subtracting TIC from TC (Lenz et al., 2021).

3.3. Biogenic silica analysis, diatom preparation and contamination assessment

Biogenic silica (BSi) analysis was performed on 0.45 g of dry sediment sampled from Co 1321. Samples were ground and analysed for BSi using the automated sequential leaching method (Müller and Schneider, 1993) at the Alfred Wegener Institute Helmholtz Centre for Polar and Marine Research (AWI Bremerhaven, Germany). Biogenic opal was calculated from BSi assuming a 10% water content within the frustule (Mortlock and Froelich, 1989; Müller and Schneider, 1993).

2 g of dry sediment from a total of 48 Holocene sediment samples with an initial biogenic opal content (Fig. 2) above 8% were processed for $\delta^{18}O_{diatom}$ analysis. The temporal resolution between two samples is about 240 years (Table 1). Diatom purification involved a multi-step procedure based on Chapligin et al. (2012a). First, sediment samples were heated to 50 °C in 35% H_2O_2 for three days to remove organic matter, before adding 10% HCl to eliminate carbonates. To separate diatoms from the detrital contaminants with higher density, samples were stepwise centrifuged in sodium polytungstate (SPT; $3Na_2WO_49WO_3{\cdot}H_2O$) heavy liquid solution of 2.50, 2.35, 2.25, 2.20 and 2.18 g cm^{-3} densities at 2500 rpm for 30 min. A few samples required additional separation steps at densities as low as 2.10 g cm^{-3}. The detritus was retained for a

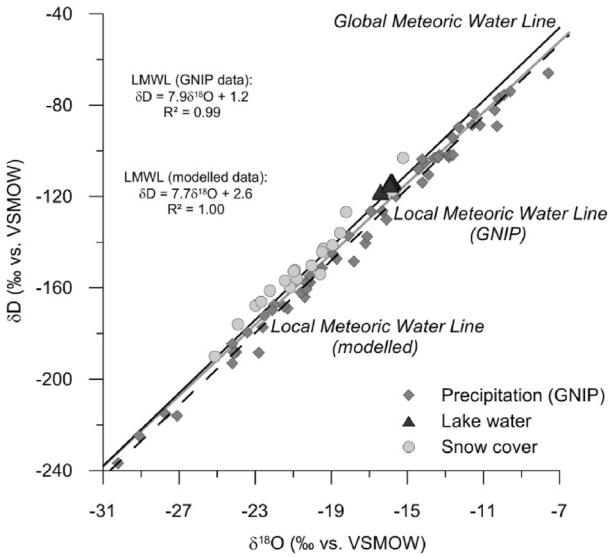

Fig. 2. $\delta^{18}O$–δD diagram for water samples from Lake Bolshoye Shchuchye and snow cover. Additionally, GNIP data for regional precipitation, the Global Meteoric Water Line (GMWL; $\delta D = 8 \cdot \delta^{18}O + 10$; Craig, 1961; Rozanski et al., 1993) and Local Meteoric Water Line (LMWL) based on GNIP data (black dash line; IAEA/WMO, 2022) and LMWL modelled from OIPC (grey solid line; Bowen, 2022) are given.

contamination assessment and $\delta^{18}O_{diatom}$ correction (Fig. S2 D). Hardly soluble micro-organic and lighter contaminants were removed by applying an inverse separation with SPT of 2.05 g cm^{-3}. Purified diatoms were then washed in ultra-pure water using a 3 μm filter and a pump system to facilitate sieving. Finally, samples were wet sieved using a Rhewum Schallfix nylon mesh and sonication system, resulting in two diatom size fractions (3–10 μm and >10 μm). Only the 3–10 μm fraction yielded sufficient material (>2 mg) to be used for $\delta^{18}O_{diatom}$ analysis.

Energy-Dispersive X-ray Spectroscopy (EDS) under a scanning electron microscope (SEM) at the German Research Centre for Geosciences (GFZ Potsdam, Germany) was used to assess contamination of all diatom samples by visual inspection (Fig. S2; A–C) and following the method introduced by Chapligin et al. (2012a). Accordingly, three replicate analyses were carried out with an excited-area size with a radius of ~200 μm at an acceleration voltage of 20.0 kV. All detectable elements were normalised to 100% weight. The results were expressed as weight percentages and displayed as oxides. The EDS data of the Lake Bolshoye Shchuchye record (Table 1; Fig. 2) indicate that all 48 purified samples contained sufficient diatom material and less than 2.5% Al_2O_3 (Chapligin et al., 2012a) to be analysed for $\delta^{18}O_{diatom}$. 32 samples were highly purified, comprising between 97.1 and 98.8% SiO_2, and 0.5–1.6% Al_2O_3, respectively. 16 samples were less pure with 94.8–96.8% SiO_2, and 1.3–2.0% Al_2O_3.

3.4. Diatom oxygen isotope analysis and $\delta^{18}O_{diatom}$ correction

The oxygen isotope composition of purified diatom samples (n = 48) and the detrital contaminant sub-samples (n = 5) were measured at the ISOLAB Facility at AWI Potsdam with a PDZ Europa 2020 mass spectrometer. All samples were measured in duplicates or triplicates (Table 1).

Prior to isotope analysis, exchangeable oxygen was removed using inert Gas Flow Dehydration (iGFD) under Argon gas at 1100 °C, after Chapligin et al. (2010). Dehydrated samples were fully reacted using laser fluorination with BrF_5 as reagent to liberate O_2 (Clayton and Mayeda, 1963) and then directly measured against an oxygen reference sample of known isotopic composition. Replicate analyses of the calibrated working standard BFC (Chapligin et al., 2011) yielded $\delta^{18}O = +28.82 \pm 0.26$‰ (n = 76) indicating an accuracy and analytical precision corresponding to the method's long-term analytical reproducibility (1σ) of ±0.25‰ (Chapligin et al., 2010).

All measured diatom $\delta^{18}O$ values were contamination-corrected using the geochemical mass-balance approach (Swann and Leng, 2009; Chapligin et al., 2012a):

$$\delta^{18}O_{corr} = \left(\delta^{18}O_{meas} - \frac{\delta^{18}O_{cont} \cdot c_{cont}}{100}\right) \Big/ \left(\frac{c_{diatom}}{100}\right) \quad (1)$$

where $\delta^{18}O_{meas}$ is the original measured $\delta^{18}O$ value of the sample. $\delta^{18}O_{corr}$ is the measured $\delta^{18}O$ value corrected for contamination, with $\delta^{18}O_{cont} = +12.5 \pm 0.6$‰ (n = 5), which represents the average $\delta^{18}O$ of the heavy detrital fractions after the first heavy liquid separation containing no diatoms (verified using SEM; Table S2; Fig. S2; D). The percentages of contamination (c_{cont}) and diatom material (c_{diatom}) within the analysed sample are calculated using the EDS-measured Al_2O_3 content of the individual sample divided by the average Al_2O_3 content of the contamination (21.5 ± 1.0% in heavy fractions, n = 5) and as (100%–c_{cont}), respectively.

3.5. Water sampling and stable water isotope analysis

During the drilling campaign, lake water samples were collected along a depth profile of the water column between the lake ice cover and bottom (n = 17), at the same location as the sediment core (Fig. 1B). Additionally, a 2.0-m snow profile was sampled from the surface of the snowpack to ground level in 10–15 cm intervals (n = 20). Snow samples were melted at room temperature. All water samples were stored cool in airtight bottles prior to stable isotope analyses.

Hydrogen (δD) and oxygen ($\delta^{18}O$) stable water isotopes were analysed at the AWI ISOLAB Facility, Potsdam, Germany with a Finnigan MAT Delta-S mass spectrometer using equilibration techniques with an analytical uncertainty (1σ) of better than ±0.8‰ for δD and ±0.1‰ for $\delta^{18}O$ (Meyer et al., 2000). The secondary parameter deuterium excess is calculated as $d = \delta D - 8 \cdot \delta^{18}O$ (Dansgaard, 1964). Data are given as per mil difference (‰) to V-SMOW and compared to the Global Meteoric Water Line (GMWL; Craig, 1961) and to the Local Meteoric Water Line (LMWL) based on Global Network for Isotopes in Precipitation (GNIP; IAEA/WMO, 2022) data of Salekhard (16 m a.s.l; situated ~150 km southeast of Lake Bolshoye Shchuchye (Fig. 1A)) as the nearest station.

3.6. Isotopic mass-balance modelling

Isotopic mass-balance modelling was performed simulating varying amount and isotopic composition of surface inflow as well as evaporative enrichment on Lake Bolshoye Shchuchye. The goal of this was to determine both the potential impact of these factors on lake water isotopic composition and the speed of the reaction.

Assuming constant lake volume and hydrological parameters, the lake water isotopic composition after a given time can be calculated according to Gonfiantini (1986):

$$\delta^{18}O_{lake} = \delta^{18}O_S - \left(\delta^{18}O_S + \delta^{18}O_0\right) * e^{-(1+mx)*\left(\frac{It}{V}\right)} \quad (2)$$

where $\delta^{18}O_0$ is the initial isotopic composition of lake water and $\delta^{18}O_S$ the steady-state composition approached over time. The latter can be expressed as:

Table 1
Main geochemical characteristics of diatoms from Lake Bolshoye Shchuchye based on EDS data. Measured $\delta^{18}O$ values ($\delta^{18}O_{meas}$), standard deviation (SD) and number of replicates (N), calculated contamination (c_{cont}; %) and $\delta^{18}O$ values corrected for contamination ($\delta^{18}O_{corr}$) are given.

Core	Sample depth (cm)	Age (cal. Ka BP)	SiO_2 (%)	Al_2O_3 (%)	Na_2O (%)	MgO (%)	K_2O (%)	CaO (%)	MnO (%)	FeO (%)	Total	$\delta^{18}O_{meas}$ (‰)	$\delta^{18}O_{meas}$ SD (‰)	N	c_{cont} (%)	$\delta^{18}O_{corr}$ (‰)
Co1321-3-SL	surface	−0.067	98.77	0.52	0.23	0.14	0.03	0.02	0.02	0.26	100.00	23.17	0.48	2	2.4	23.44
Co 1321-2	4.4	−0.010	98.57	0.48	0.55	0.12	0.01	0.05	0.05	0.17	100.00	23.41	0.23	2	2.2	23.66
Co 1321-2	20.9	0.221	98.02	0.71	0.63	0.20	0.01	0.05	0.03	0.36	100.00	24.73	0.03	2	3.3	25.15
Co 1321-2	35.8	0.461	98.76	0.51	0.37	0.11	0.00	0.02	0.03	0.22	100.00	25.06	0.49	2	2.4	25.36
Co 1321-2	54.1	0.789	97.44	0.86	1.04	0.15	0.03	0.05	0.06	0.39	99.99	26.15	0.15	2	4.0	26.71
Co 1321-2	67.8	1.047	97.98	0.88	0.46	0.16	0.01	0.07	0.01	0.43	100.00	24.51	0.12	2	4.1	25.02
Co 1321-31-II	97.9	1.602	96.65	1.49	0.86	0.21	0.09	0.08	0.02	0.61	100.00	23.61	0.14	2	7.2	24.48
Co 1321-31-II	112.4	1.851	97.85	0.78	0.69	0.16	0.02	0.04	0.06	0.40	100.00	29.22	0.33	2	3.6	29.85
Co 1321-32-I	152.7	2.515	98.21	0.53	0.79	0.14	0.00	0.02	0.05	0.27	100.00	24.89	0.22	3	2.5	25.20
Co 1321-32-I	167.7	2.761	98.14	0.85	0.38	0.17	0.01	0.06	0.02	0.39	100.00	28.06	0.21	2	3.9	28.70
Co 1321-32-I	187.5	3.080	98.01	0.75	0.66	0.15	0.02	0.03	0.04	0.35	100.01	27.71	0.25	2	3.5	28.26
Co 1321-32-I	200.6	3.287	95.14	1.47	2.58	0.10	0.14	0.13	0.03	0.41	100.00	24.47	0.07	2	6.8	25.35
Co 1321-32-I	215.4	3.514	97.89	0.81	0.60	0.18	0.01	0.09	0.04	0.38	100.00	25.16	0.15	2	3.8	25.65
Co 1321-32-II	235.2	3.808	97.58	1.09	0.65	0.13	0.07	0.05	0.09	0.35	100.00	26.43	0.23	2	5.1	27.17
Co 1321-32-II	249.8	4.018	98.04	0.74	0.75	0.10	0.01	0.05	0.08	0.25	100.00	27.37	0.09	2	3.4	27.89
Co 1321-32-II	265.8	4.242	98.09	0.85	0.49	0.16	0.01	0.05	0.02	0.34	100.00	25.29	0.08	2	3.9	25.81
Co 1321-32-II	281.8	4.459	97.50	0.97	0.81	0.15	0.04	0.07	0.04	0.43	100.00	25.05	0.25	2	4.5	25.64
Co 1321-32-II	298.1	4.678	97.73	0.65	1.19	0.03	0.03	0.13	0.05	0.20	100.00	25.84	0.12	3	3.0	26.25
Co 1321-32-II	314.5	4.889	96.01	1.89	0.93	0.30	0.18	0.06	0.01	0.63	100.01	26.84	0.04	2	8.8	28.22
Co 1321-32-II	330.3	5.090	97.89	0.89	0.66	0.09	0.02	0.03	0.02	0.40	99.99	26.83	0.04	2	4.1	27.45
Co 1321-33-I	353.6	5.382	97.76	0.96	0.74	0.11	0.02	0.04	0.03	0.34	99.99	26.31	0.25	2	4.5	26.96
Co 1321-33-I	368.6	5.565	96.58	1.53	0.92	0.21	0.09	0.09	0.02	0.56	100.00	26.15	0.11	2	7.1	27.19
Co 1321-33-I	400.9	5.954	98.18	0.82	0.45	0.12	0.04	0.11	0.04	0.24	100.00	25.62	0.11	2	3.8	26.14
Co 1321-33-I	425.6	6.243	96.45	1.87	0.50	0.34	0.14	0.08	0.03	0.59	100.00	27.51	0.06	2	8.7	28.94
Co 1321-33-II	434.8	6.350	96.83	1.26	1.15	0.17	0.06	0.06	0.04	0.45	100.00	30.70	0.21	3	5.9	31.83
Co 1321-33-II	450.8	6.534	97.16	1.25	0.85	0.14	0.02	0.08	0.04	0.47	100.00	25.87	0.13	2	5.8	26.69
Co 1321-33-II	465.9	6.705	97.98	1.00	0.28	0.14	0.06	0.07	0.03	0.43	100.00	26.09	0.04	2	4.6	26.75
Co 1321-33-II	483.1	6.899	98.12	0.89	0.26	0.15	0.05	0.07	0.04	0.40	100.00	28.61	0.18	2	4.2	29.31
Co 1321-33-II	499.1	7.077	96.04	1.69	1.46	0.08	0.15	0.11	0.02	0.46	100.00	25.53	0.19	2	7.9	26.64
Co 1321-33-II	534.5	7.466	97.09	1.35	0.94	0.13	0.04	0.05	0.01	0.39	100.00	25.71	0.07	2	6.3	26.60
Co 1321-34-I	555.1	7.689	97.78	0.95	0.49	0.14	0.01	0.08	0.04	0.51	100.00	27.44	0.25	2	4.4	28.13
Co 1321-34-I	572.6	7.878	97.76	0.82	0.72	0.06	0.01	0.07	0.02	0.55	100.00	26.61	0.04	2	3.8	27.17
Co 1321-34-I	585.3	8.014	97.63	1.01	0.77	0.13	0.02	0.07	0.03	0.36	100.00	28.14	0.06	2	4.7	28.91
Co 1321-34-I	602.8	8.200	97.31	0.99	1.10	0.03	0.03	0.08	0.04	0.42	100.00	25.24	0.16	2	4.6	25.85
Co 1321-34-I	617.6	8.357	97.16	1.12	0.81	0.15	0.09	0.18	0.05	0.45	100.00	25.74	0.18	2	5.2	26.46
Co 1321-34-II	667.6	8.882	97.96	1.09	0.37	0.14	0.03	0.14	0.01	0.26	100.00	25.77	0.04	2	5.1	26.48
Co 1321-34-II	684.7	9.061	96.05	1.93	1.01	0.30	0.12	0.08	0.07	0.41	99.95	26.58	0.06	2	9.0	27.97
Co 1321-34-II	698.6	9.205	97.49	1.32	0.36	0.17	0.11	0.10	0.04	0.42	100.00	26.95	0.11	2	6.1	27.90
Co 1321-34-II	713.1	9.355	96.50	0.92	2.15	0.07	0.02	0.12	0.00	0.23	100.00	26.36	0.37	2	4.3	26.98
Co 1321-35-I	768.9	9.928	97.26	1.62	0.29	0.21	0.14	0.14	0.03	0.32	100.00	26.24	0.03	2	7.5	27.36
Co 1321-35-I	778.4	10.025	98.24	1.05	0.13	0.12	0.03	0.14	0.00	0.30	100.00	25.92	0.08	2	4.9	26.61
Co 1321-35-I	787.4	10.118	96.13	1.97	0.62	0.35	0.14	0.15	0.05	0.59	100.00	25.49	0.20	3	9.2	26.81
Co 1321-35-I	802.3	10.270	95.51	1.74	2.08	0.09	0.18	0.08	0.04	0.29	100.00	25.16	0.24	3	8.1	26.28
Co 1321-35-I	817.0	10.420	96.46	1.83	0.50	0.29	0.17	0.20	0.02	0.53	100.00	26.78	0.06	2	8.5	28.12
Co 1321-35-I	835.3	10.606	96.68	1.77	0.74	0.22	0.07	0.07	0.03	0.42	100.00	26.49	0.16	2	8.3	27.75
Co 1321-35-II	851.3	10.768	96.01	2.00	0.65	0.37	0.16	0.18	0.05	0.56	100.00	25.30	0.16	2	9.3	26.62
Co 1321-35-II	872.4	10.981	96.21	2.02	0.55	0.27	0.17	0.23	0.06	0.50	100.00	25.86	0.27	2	9.4	27.25
Co 1321-35-II	915.2	11.411	94.76	1.99	2.20	0.21	0.12	0.17	0.07	0.48	100.00	26.43	0.31	2	9.3	27.86

$$\delta^{18}O_S = \frac{\delta^{18}O_I + mx\delta^{18}O^*}{1 + mx} \quad (3)$$

The limiting isotope enrichment $\delta^{18}O^*$ is calculated according to Gat (1981), m and x represent the temporal enrichment slope and the fraction of lake water lost by evaporation, respectively. For further elaboration on this approach, we refer to Darling et al. (2006) and references therein. The inflow isotopic composition $\delta^{18}O_I$ was assumed to be equal to $\delta^{18}O_0$ and to $\delta^{18}O$ of mean annual precipitation (−17.8‰). Mean annual precipitation and mean summer precipitation were modelled using the Online Isotopes in Precipitation Calculator (OIPC; Bowen, 2022), c.f. chapter 4.2. Since data for evaporation are not readily available, the amount of evaporation from the lake surface was approximated as a function of summer mean air temperature T, atmospheric humidity h, altitude a and latitude A (Linacre, 1977).

$$E_0 = \frac{700\frac{T_m}{100-A} + 15(T - T_d)}{(80 - T)}\left(\frac{mm}{d}\right) \quad (4)$$

where $T_m = T + 0.006a$ and the dew-point T_d is approximated according to Lawrence (2005) as $T_d \approx T - \left(\frac{1-h}{5}\right)$. Assuming an ice-free period of 100 days per year, the calculated daily evaporation rates were multiplied by 100 to obtain annual values. The isotopic composition of atmospheric moisture was calculated according to Gibson et al. (1999) based on summer precipitation.

3.7. Chironomid analysis

Eighty-four samples were prepared for chironomid analysis with standard techniques (Brooks et al., 2007). Chironomid identification followed Wiederholm (1983) and Brooks et al. (2007).

The ratio of lotic (moving water or riverine) and lentic (standing

water) chironomid taxa in sediments of Lake Bolshoye Shchuchye, and chironomid-inferred mean July air temperature (T_{air}) are in the focus of this study. In this context, increasing representation of the lotic fauna reflects stronger runoff and more intensive water input with the inflowing rivers (Nazarova et al., 2017c; Biskaborn et al., 2019). For information on ecology of chironomid taxa, we refer to Brooks et al. (2007), Stief et al. (2005), Moller Pilot (2009, 2013), and Nazarova et al. (2011, 2015, 2017a, b). The reconstruction of mean July air temperatures was performed using the North Russian (NR) chironomid-based temperature inference model (WA-PLS, 2 component; r^2 boot = 0.81; RMSEP boot = 1.43 °C; Nazarova et al., 2015). Chironomid-based reconstruction was performed in C2 version 1.7.7. (Juggins, 2007).

3.8. Digital elevation model preparation and delineation of the lake catchment

The freely distributed digital elevation model (DEM) ArcticDEM (Porter et al., 2018) was used for the Lake Bolshoye Shchuchye catchment delineation and morphometric analysis of the catchment. Raw 10-m resolution ArcticDEM data covering the area of interest were downloaded from the Polar Geospatial Center data portal (https://www.pgc.umn.edu/data/arcticdem/). Contours at 20-m intervals were extracted from the DEM and were manually corrected for artefacts and missing patches in order to build up a hydrologically correct digital terrain model (DTM). This improved DTM was created by interpolating corrected contours using the TopoToRaster algorithm with drainage enforcement (Hutchinson, 1989) within the ESRI© ArcGIS 10.2 software. The catchment of Lake Bolshoye Shchuchye was extracted based on the hydrologically correct topographic representation within QGIS 3.10 software. For morphometric analysis, topographic variables were obtained, including slopes, aspects, total curvature, flow direction, flow accumulation. All topographic variables were calculated with R (R Core Team, 2017) using the packages 'raster' (Robert and van Etten, 2012), 'dynatopmodel' (Quinn et al., 1995) and 'spatialEco' (Evans, 2020).

3.9. Calculation of the snow water equivalent within the catchment

The catchment polygon was further used to analyse the distribution of snow depth and snow water equivalent (SWE). Snow depth within the lake catchment at 10-m resolution was calculated using auxiliary data: cumulative snow probability for snowmelt period of 2019 extracted from Sentinel-2 time series and snow depth ranges (0–845 cm of snow) measured within ten snow survey profiles within the neighboring Lake Bolshaya Khadata catchment (Gokhman and Zhidkov, 1979). The atmospherically corrected (sen2cor, ESA) Sentinel-2 Level-2A data archive was analysed in order to calculate the cumulative snow probability value for the entire catchment. Level-2A data provide the snow probability band scaled from 0 to 1 based on the specific spectral signature of snow cover, where values of 0 and 1 correspond to 0% snow and 100% snow, respectively. For the 2019 glaciological year (October–May; Ivanov, 2013), we obtained all images (less than 20% clouds) and filtered out all scenes covering less than 85% of the lake catchment without clouds. Further, all snow probability bands of these images were summarised to calculate a cumulative value: there were seven scenes meeting the requirements covering the period from May 8, 2019 (maximum of snow) to July 25, 2019 (quasi-complete melting of snow). Within the range of cumulative snow probability, the range of snow depth was scaled to measured snow depths of the neighboring catchment in 1978 (Gokhman and Zhidkov, 1979). The SWE was calculated based on the empirical relationship between snow depth and SWE obtained for tundra landscape in Central Yamal (500 km to the North from the lake) according to Dvornikov et al. (2015). All satellite image analysis and calculations were performed within Google Earth Engine Cloud Computing platform (Gorelick et al., 2017).

4. Results

4.1. Stable water isotopes

The results of stable water isotope analyses are presented in a $\delta^{18}O$–δD diagram (Fig. 2). One water sample taken directly at the ice-water boundary (Fig. 3A) and one surface snow sample (Fig. 3C) were excluded from interpretation due to significantly different isotopic signals from those for other samples; likely due to interaction between water phases. The average recent water isotope composition of Lake Bolshoye Shchuchye is −15.9 ± 0.2‰ for $\delta^{18}O_{lake}$, −114.4 ± 2.6‰ for δD_{lake} and +13.0 ± 0.5‰ for *d* excess (n = 16) representing spring conditions under lake ice. The water column $\delta^{18}O$-profile reveals no substantial changes with depth (Fig. 3A). Small variations of 0.5‰ were detected at 10 m depth, incoherent with T_{lake} changes (Fig. 3B). A positive (0.08‰/°C), but statistically not significant (R^2 = 0.14) correlation was found between $\delta^{18}O_{lake}$ and T_{lake}.

The snow cover displays a large variability between single layers in their $\delta^{18}O_{snow}$ and δD_{snow} values ranging from −25.1 to −15.2‰ and from −190.1 to −103.1‰, respectively. The *d* excess ranges from +2.7 to +18.9‰. The minimum $\delta^{18}O_{snow}$ with −25.1‰ is reached at the depth of 115 cm $\delta^{18}O_{snow}$ values demonstrate a continuous decrease of ~0.07‰/cm in the lower (195–115 cm) part of the column (Fig. 3C). Visible variations in $\delta^{18}O_{snow}$ with smaller maxima at depths of 10, 75 and 105 cm occur in the upper section (115–0 cm) of the core. In general, this interval displays a gradual increase of ~0.09‰.cm^{-1} in $\delta^{18}O_{snow}$ values.

As precipitation samples could not be collected at Lake Bolshoye Shchuchye, mean annual $\delta^{18}O_{prec}$ and δD_{prec} values of regional precipitation have been derived from the GNIP database (IAEA/WMO, 2022) for Salekhard (Fig. 1A). Additionally, $\delta^{18}O_{prec}$ and δD_{prec} values as well as a LMWL were modelled for the drilling location based on the algorithm published by Bowen and

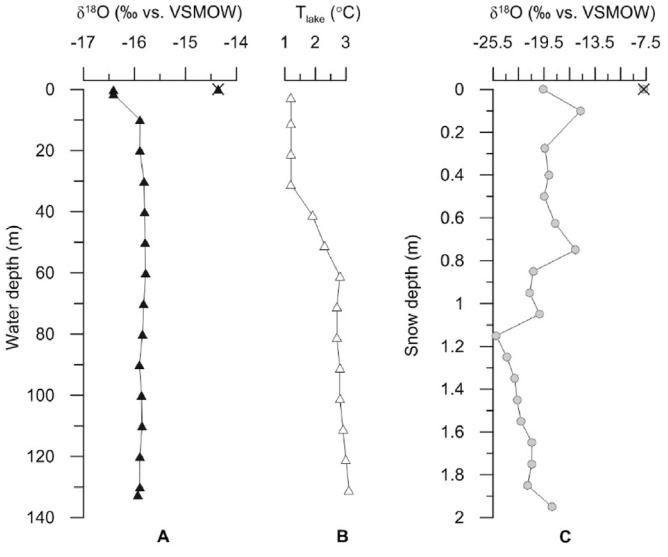

Fig. 3. Depth profiles. (A) Oxygen isotope composition of water from Lake Bolshoye Shchuchye. (B) Lake water temperature, measured 50 m north of the coring site. (C) Oxygen isotope composition of snow cover. Water and snow samples excluded from interpretation are marked as crossed out signs.

Revenaugh (2003) and Bowen et al. (2005) using the OIPC (Bowen, 2022). Modelled $\delta^{18}O_{prec}$ and δD_{prec} values of −17.8 ± 0.4‰ and −135.0 ± 3.0‰ (Bowen, 2022) are consistent with GNIP values of −17.5 ± 1.7‰ and −136.1 ± 13.2‰, respectively (IAEA/WMO, 2022). The LMWL based on modelled values was determined as: $\delta D = 7.7\ \delta^{18}O + 2.6‰$ ($R^2 = 1.00$; Fig. 3; Bowen, 2022) and is in a good agreement with the LMWL from GNIP data (IAEA/WMO, 2022) with a slope of 7.9 and an intercept of +1.2‰ ($R^2 = 0.99$; Fig. 3). Minor offsets between the LMWLs are mainly due to differences in both temporal and spatial domains. Due to the distance of Salekhard to the sampling location, we assume the modelled $\delta^{18}O_{prec}$ and δD_{prec} values and the LMWL to be more reliable for Lake Bolshoye Shchuchye.

4.2. Oxygen isotope record

The Lake Bolshoye Shchuchye diatom $\delta^{18}O_{corr}$ values (further referred to as $\delta^{18}O_{diatom}$) range from +23.4‰ to +31.8‰ (Fig. 4; Table 1) and exhibit the same trend as $\delta^{18}O_{meas}$ values. Contamination correction leads to an offset of $\delta^{18}O_{corr}$ towards higher values of about 0.7‰ in the upper part of the core (younger than 8.5 cal Ka BP) and 1.3‰ higher for the lower part (older than 8.5 cal Ka BP). The mean standard deviation of $\delta^{18}O_{diatom}$ of all samples is 0.16 ± 0.11‰ and the maximum standard deviation of duplicates is ±0.37‰ (Table 1).

The Co 1321 core is characterised by a mean $\delta^{18}O_{diatom}$ value of +27.0‰ for the complete Holocene. In Early Holocene (11.4–7 cal Ka BP), the $\delta^{18}O_{diatom}$ values are with +27.3 ± 0.8‰ slightly higher than the Holocene mean. Highest mean $\delta^{18}O_{diatom}$ values with +27.9 ± 2.0‰ are observed in Mid Holocene (7–5 cal Ka BP), whereas lowest $\delta^{18}O_{diatom}$ values of +26.3 ± 1.7‰ characterise the Late Holocene (5 cal Ka BP to present). The maximum $\delta^{18}O_{diatom}$ value (+31.8‰) in the record is registered at 6.3 cal Ka BP. The absolute minimum in the $\delta^{18}O_{diatom}$ record occurs at the sediment surface at 0.0 cal Ka BP with +23.4‰. Sharp variations are observed every ~0.7–1.5 cal Ka with smaller maxima at 0.8, 1.9, 2.8, 4.0, 4.9, 6.4, 6.9, 8.1, 9.1, 10.0 and 10.4 cal Ka BP and smaller minima at 1.6, 2.4, 3.3, 4.5, 5.9, 6.5, 7.5, 8.3, 10.3 and 10.8 cal Ka BP. In general, a gradual depletion of ~0.39‰/1000 years is observed between 10.9 and 0.0 cal Ka BP (Fig. 4).

4.3. Chironomids

The chironomid fauna of Lake Bolshoye Shchuchye is dominated by cold-tolerant lentic taxa usual for Arctic lakes. Several taxa characteristic for lotic environments have been found in the lake sediments. Among them are taxa from the subfamilies Diamesinae (e.g. *Diamesa aberrata*-type, *D. cinerella*-type, *D. bertrami*-type), that usually inhabit small, cold running streams and brooks and Orthocladiinae (e.g. *Eukiefferiella*, *Metriocnemus*, *Thienemanniella clavicornis*-type, *Tvetenia bavarica*-type), that occur in flowing waters and surf zones of lakes.

Representation of the lotic taxa varies considerably reaching 50% of the fauna during Early Holocene (at ~10.6 cal Ka BP) (Fig. 4). However, rather high concentration of lotic chironomids (25–33% of the fauna) is observed between 7.7 and 4.5 cal Ka BP. Between 4.5 and 3.2 cal Ka BP, no lotic taxa appear in the lake, indicating a decrease of the water inflow (Fig. 4). At 3.2 cal Ka BP, lotic

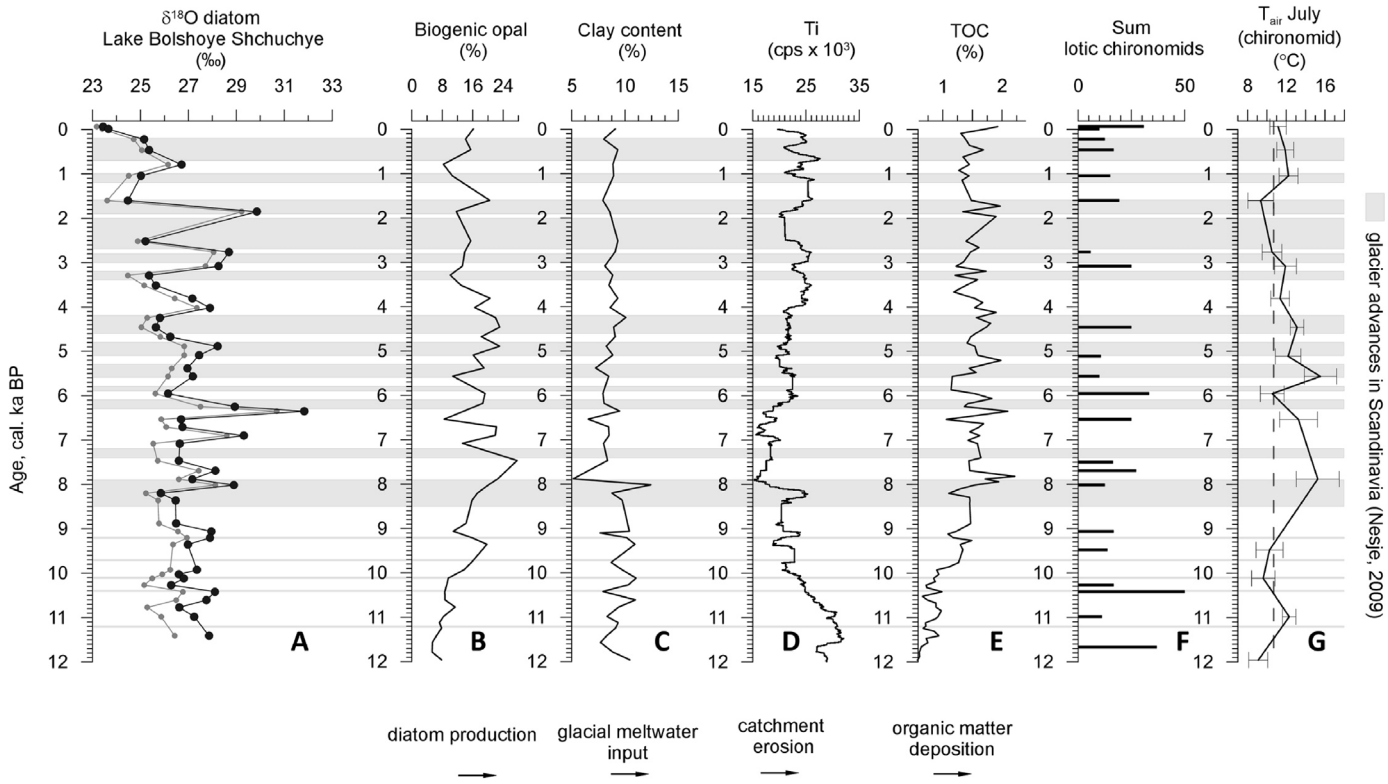

Fig. 4. (A) Holocene oxygen isotope composition of diatoms from Lake Bolshoye Shchuchye (grey raw data: $\delta^{18}O_{meas}$; black: contamination-corrected $\delta^{18}O_{corr}$ values, referred to as $\delta^{18}O_{diatom}$) compared to other lake internal parameters, such as: (B) the biogenic silica percentage, as proxy for the diatom production, (C) clay content, as glacial meltwater proxy, (D) Ti cps (counts per second), a proxy for detrital input and catchment erosion. (E) TOC content, as proxy for organic matter input to the lake, as well as (F) the sum of lotic chironomids, indicative for riverine influx, and (G) a chironomid-based July air temperature reconstruction for Lake Bolshoye Shchuchye. The dashed line corresponds to the modern mean July air temperature (of 10.6 °C). All lake internal proxies are introduced and discussed in detail in Lenz et al. (2021). Greyscales indicate periods of known glacier advances in Scandinavia (Nesje, 2009).

chironomids appear in the lake again and their abundance reaches 25% of the fauna. Between 3.2 and 0 cal Ka BP, the abundance of lotic taxa remains at 11% on average, and it rises to 31% towards the modern times.

The chironomid-based reconstructed T_{air} during Early Holocene are on average ~1.5 °C below modern level. The transition to Mid Holocene is characterised by an increase in chironomid abundances with a gradual rise in the reconstructed T_{air} to the modern level (10.6 °C). Between ~8.0 and 3.2 cal Ka BP, the T_{air} are the highest and reach up to 3 °C above the present T_{air} at 5.5 cal Ka BP. However, there is a cooling tendency in T_{air} after 5.5 cal Ka BP, when reconstructed T_{air} gradually decrease and reach ~1 °C below the modern T_{air} at ~1.7 cal Ka BP. Chironomid-based reconstructed T_{air} are slightly above modern values between 1.0 and 0.6 cal Ka BP, subsequently decreasing to the present level. The standard error for the chironomid-based T_{air} reconstruction is 1.2 ± 0.4 °C for the Holocene.

5. Discussion

5.1. Isotope hydrology

When interpreting lacustrine $\delta^{18}O_{diatom}$ records, a proper understanding of the modern hydrology is a precondition for assessing possible past hydrological changes.

The recent mean Bolshoye Shchuchye $\delta^{18}O_{lake}$ of −15.8‰ is slightly higher than the regional $\delta^{18}O_{prec}$ of −17.8‰ (Bowen, 2022). Additionally, the lake water isotope samples plot on the GMWL and slightly above the modelled LMWL (Fig. 2) and follow a linear dependency with a slope of 7.2 and an intercept of +0.3 ($R^2 = 0.90$; $n = 16$). This suggests that $\delta^{18}O_{lake}$ roughly corresponds to $\delta^{18}O_{prec}$, slightly shifted to more positive values probably due to seasonality effects.

At the same time, water samples are situated close to the GMWL (Fig. 2), indicating the absence of major evaporation effects in recent times. The V-shape of the lake basin, almost completely surrounded by steep slopes, allows for lake level fluctuations without significant changes in the lake surface area and water volume.

Palaeogeographical and geomorphological studies yielded pre-Holocene Bolshoye Shchuchye lake level fluctuations with a high-stand 8 m above present lake level along parts of the western shore (Svendsen et al., 2019). This higher than modern lake level might have resulted from intense meltwater influx from contemporaneous glaciers in the lake catchment and a simultaneous damming of the lake by a glaciofluvial fan at the south outlet until around 14–15 cal Ka BP (Svendsen et al., 2019). The lake level dropped when this fan was incised by glacial meltwaters (Regnéll et al., 2019). Additionally, seismic profiles point to lower lake levels prior to 15 cal Ka BP (Haflidason et al., 2019). A terrace in the northern part of Lake Bolshoye Shchuchye documents a 2–3 m higher lake level at ~2–3 cal Ka BP (Svendsen et al., 2019). Therefore, lake level changes and associated evaporation effects cannot be fully excluded at Lake Bolshoye Shchuchye, especially during the Last Glacial Maximum and the early deglaciation period, but are assumed to be weak for the Holocene, the period of interest.

The water $\delta^{18}O_{lake}$ depth profile shows a constant isotope composition (Fig. 3A) and suggests a well-mixed water column lacking any isotopic stratification, at least during spring 2016. There is no notable relationship between $\delta^{18}O_{lake}$ and T_{lake} (Fig. 3A and B). Hence, water column temperature effects are assumed to be of minor importance on $\delta^{18}O_{lake}$.

The snow cover isotope samples plot on or close to the GMWL (Fig. 2) in the co-isotope diagram with a slope of 7.9 and an intercept of +10.8 ($R^2 = 0.96$). The mean $\delta^{18}O_{snow}$ of −20.4‰ (*d* excess = +12.9‰) is slightly higher than the regional mean $\delta^{18}O_{prec}$ of −22.8‰ (*d* excess = +8.4‰) between October and April (when precipitation falls as snow) derived from the OIPC (Bowen, 2022). This likely represents a seasonal bias towards late winter and spring snow, but could also include effects of sublimation, evaporation and wind drift processes altering the snow pack's isotopic composition over time (Friedman et al., 1991; Nikolaev and Mikhalev, 1995). The $\delta^{18}O_{snow}$ profile displays variations with depth (Fig. 3C) which might be associated with isotopic differences between individual precipitation (or deposition) events persisting despite snow metamorphism (Friedman et al., 1991). Nevertheless, as T_{air} is a primary control of $\delta^{18}O_{prec}$ especially in polar regions (Dansgaard, 1964), it is likely that the isotopically lightest layers (110–130 cm) with $\delta^{18}O_{snow}$ of −24 to −25‰ were formed during the coldest months (January–February). Generally, it can be concluded that snow can be a source of isotopically-depleted water draining into the lake.

In summary, Lake Bolshoye Shchuchye is a well-mixed, non-evaporative and isotopically rather uniform lake, which is mainly fed by meteoric waters, i. e. precipitation with an important contribution of melting snow from higher altitudes. Although there are indications of evaporation effects in the past, we suggest the precipitation signal ($\delta^{18}O_{prec}$) to be most relevant for $\delta^{18}O_{lake}$.

5.2. Isotope fractionation and main controls on $\delta^{18}O_{diatom}$

Variations in $\delta^{18}O_{diatom}$ values of lacustrine sediment are mainly controlled by changes in water temperature (T_{lake}) and/or the corresponding $\delta^{18}O_{lake}$ (Labeyrie, 1974; Juillet-Leclerc and Labeyrie, 1987; Leng and Barker, 2006; Dodd and Sharp, 2010).

When comparing the overall Holocene average Lake Bolshoye Shchuchye $\delta^{18}O_{diatom}$ of +27.0‰ with the recent average $\delta^{18}O_{lake}$ of −15.9‰, a fractionation coefficient $\alpha_{(silica\text{-}water)} = (1000 + \delta^{18}O_{diatom})/(1000 + \delta^{18}O_{lake})$ (Juillet-Leclerc and Labeyrie, 1987) of 1.0436 was determined. This yields an isotopic enrichment $\Delta^{18}O_{SiO2-H2O} = 42.9‰$ corresponding to a T_{lake} of 4.5 °C that matches well the blooming temperature of the diatom species *Aulacoseira subarctica* (~4 °C; Gibson et al., 2003; Lepskaya et al., 2010). In the sediments of the lake, *A. subarctica* is dominant from 50 to 60% in the beginning of the Holocene to 80–95% throughout the Holocene until recently (A. Ludikova, pers. comm.; Fig. S2). This suggests that the $\delta^{18}O_{diatom}$ values at Lake Bolshoye Shchuchye (Table 1) are the right order of magnitude and, consequently, underline the general applicability of the diatom oxygen isotope signal for palaeoreconstructions at the lake.

To test whether temperature effects are the dominant forcing responsible for the short-term variability in $\delta^{18}O_{diatom}$ of up to 5‰, we calculated a scenario function displaying possible changes in T_{air} and T_{lake}. The aforementioned $\delta^{18}O_{diatom}$-temperature coefficient of −0.2‰/°C (Dodd and Sharp, 2010) and the regional temperature relation between monthly mean $\delta^{18}O_{prec}$ and T_{air} of +0.34‰/°C (Salekhard; IAEA/WMO, 2021) were used. The scenario function for a 5‰-shift as visible in the Bolshoye Shchuchye diatom oxygen isotope record constitutes a linear function, the slope of which is defined by the quotient of the T_{lake} and T_{air} coefficients (Fig. S3). Intercept and Zero of the function represent "traditional" interpretations of temperature effects regarding either T_{lake} or T_{air} alone, respectively. The former suggests a drop in T_{lake} of 25 °C while the latter corresponds to a rise in T_{air} of 14.7 °C needed to explain the shifts of 5‰ in $\delta^{18}O_{diatom}$. Due to the fact that present lake temperature changes in the course of an annual cycle amount to 7–11 °C only (Mitrofanova, 2017; Vinokurova, 2017; Regnéll et al., 2019), variations of 25 °C during the summer period (diatom bloom) are highly unlikely. Consequently, T_{lake} alone cannot be the primary control and rather plays a subordinate role in

explaining $\delta^{18}O_{diatom}$ in Lake Bolshoye Shchuchye. Similarly, a 14.7 °C increase in T_{air} is unlikely and contrasts with only ~3–4 °C from pollen reconstructions (Andreev et al., 2005) and maximum 6 °C from the current chironomid-based reconstruction for the complete Holocene (Fig. 4). Other mathematically possible combinations of T_{air} and T_{lake} (points plotting on the scenario function) are not plausible either as they would require even more pronounced changes of T_{air} and T_{lake}.

Since Lake Bolshoye Shchuchye currently does not show evaporative enrichment, we conclude the isotopic composition of the inflow to be the main driver of the lake water isotopic composition and, hence, of the $\delta^{18}O_{diatom}$ record. Inflow, in turn, largely reflects precipitation, but with temperature effects ruled out as the single decisive factor, such changes can only be attributed to atmospheric circulation changes or hydrological processes within the lake's catchment.

Reorganization of the atmospheric transport patterns in Early Holocene after the decay of the Eurasian Ice Sheet around ~10 cal Ka BP, allowing moisture from the North Atlantic to enter the region, is in line with the northward migration of the treeline. Forest conditions persisted in the catchment until ~4 cal Ka BP, when the treeline retreated back south (Clarke et al., 2020). Today, westerly/northwesterly cyclones originating over the Atlantic (the Northern and Norwegian seas) moving across Scandinavia to the Taymyr Peninsula bring relatively warm and moist air masses to the Polar Urals year-round, especially in winter (Kononov et al., 2005; Shahgedanova et al., 2012; Pischalnikova, 2016). Relatively cold northerly cyclones forming around the Novaya Zemlya archipelago over the Barents and Kara seas deliver comparably less moisture (Kononov et al., 2005; Morozova et al., 2006). However, this northerly influence might have increased over the Holocene with a reduced sea ice concentration in the Kara and Barents Sea sectors. Moreover, recycled moisture from regional terrestrial surface waters might contribute through evaporation/evapotranspiration in summer (Bonne et al., 2020) in line with the establishment of forests in the catchment. Changes in the relative contribution of these moisture sources to the local water balance can therefore shift $\delta^{18}O_{lake}$ and $\delta^{18}O_{diatom}$ both towards higher and lower $\delta^{18}O$ values. Relative changes of the moisture sources and associated changes in precipitation intermittency should be visible in regional palaeoenvironmental reconstructions.

In summary, the changes in the Lake Bolshoye Shchuchye $\delta^{18}O_{diatom}$, are mainly driven by changes in $\delta^{18}O_{lake}$ signal, affected by T_{air}, atmospheric circulation and local hydrological conditions.

5.3. The Bolshoye Shchuchye $\delta^{18}O_{diatom}$ record

The diatom oxygen isotope record displays higher overall values of +27.4 ± 1.3‰ in Early-to Mid-Holocene (with the absolute maximum $\delta^{18}O_{diatom}$ of +31.8‰ at 6.4 cal Ka BP) and lower values of +26.4 ± 1.7‰ in Mid-to Late Holocene (with a clear minimum of +23.2‰ at the surface corresponding to the most recent, ~100 years old sediments). Generally, a gradual decrease in $\delta^{18}O_{diatom}$ of ~3–4‰ over the Holocene is notable in the Bolshoye Shchuchye $\delta^{18}O_{diatom}$ record, especially when considering the minima (Fig. 4). This is in line with the summer insolation decrease at 60°N (Berger and Loutre, 1991). Insolation reaches a maximum in Early Holocene and a minimum in Late Holocene, i.e. during the Little Ice Age (LIA). The high overall variability in the Bolshoye Shchuchye $\delta^{18}O_{diatom}$ record ($\Delta^{18}O$ of 8.6‰) results from both this trend with higher $\delta^{18}O_{diatom}$ values in the first half of the Holocene and lower values in Late Holocene as well as short-term fluctuations superimposed upon this trend.

These fluctuations consist of short term (centennial-scale) maxima and minima of more than 5‰, setting the Bolshoye Shchuchye $\delta^{18}O_{diatom}$ record apart from most other diatom oxygen isotope records stemming from high-latitude open lakes. Since these variations in $\delta^{18}O_{diatom}$ are in most cases based on more than one data point they are unlikely to be artefacts related to sample preparation or contamination correction issues.

The key questions are (1) which processes may be responsible for these short-term variations in $\delta^{18}O_{diatom}$ and (2) whether these processes are related to a larger scale pattern, visible in other lake-internal proxies and beyond or rather singular observations for Lake Bolshoye Shchuchye.

Generally, high-latitude lacustrine diatom oxygen isotope records from open lakes are rather smooth depending on depth, volume and residence time of the lake under consideration (Swann et al., 2010; Chapligin et al., 2012b; Kostrova et al., 2019, 2021). These records vary usually by 3–5‰ over the entire Holocene and have been interpreted taking into account the individual hydrological situation and isotopic background of each lake. As a consequence, short-term fluctuations rarely exceed 2‰ and have been found (but not interpreted) as single-point maxima in Lake Kotokel, a very shallow, highly evaporative lake located near Lake Baikal (Kostrova et al., 2013, 2014). Moreover, two short-term minima of 4–5‰ have been described in only one published $\delta^{18}O_{diatom}$ record, at 4.7 and 1.4 cal Ka BP for Lake Chuna on the Kola Peninsula (Jones et al., 2004).

Isotopic mass-balance modelling (Fig. 5) shows the potential impact of evaporative enrichment on Lake Bolshoye Shchuchye for three different scenarios, ranging from present conditions to hypothetic much lower annual precipitation and atmospheric humidity. While evaporation can indeed impart an effect of ~2‰ within several decades, it fails to reproduce the magnitude of the short-term fluctuations observed in the Lake Bolshoye Shchuchye record. The difference between present-day conditions (precipitation 610 mm a^{-1}, h = 0.9) and the most arid, hypothetic scenario (200 mm a^{-1}, h = 0.7) amounts to an isotopic enrichment of only 1.85‰. These results, in conjunction with the fact that Lake Bolshoye Shchuchye currently does not exhibit an evaporative signature, suggest that there must be a different locally-confined influence on the water isotope composition to explain the minima

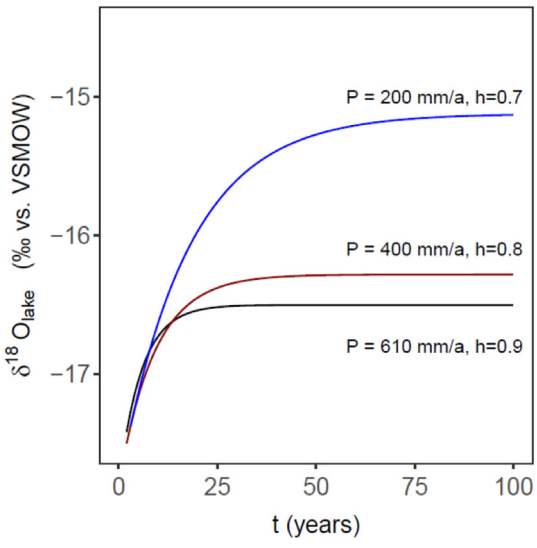

Fig. 5. Modelled evaporative enrichment of lake water over time for three different scenarios of precipitation and atmospheric humidity. The black line represents present-day precipitation (P) and humidity (h) level, whereas the blue and red lines characterise hypothetical conditions with much lower precipitation and humidity. (For interpretation of the references to colour in this figure legend, the reader is referred to the Web version of this article.)

and maxima in the $\delta^{18}O_{diatom}$ record.

Large-scale atmospheric patterns (i.e. shifts in the moisture transport and precipitation regime, seasonality of precipitation) seem unlikely as they would have an influence on a larger region that should be visible in other local proxies (Fig. 4) and regional datasets (Fig. 7; cf. chapter 5.5) as well and would lead to rather moderate changes. Shemesh et al. (2001) attributed an overall decreasing trend in $\delta^{18}O_{diatom}$ over the Holocene to the enhanced influence of Arctic continental air masses (with light isotope signature) after the decay of the Eurasian Ice Sheet. A decrease in diatom oxygen isotope record at Yellowstone Lake, USA was related to an amplified seasonal cycle of insolation during the Holocene (Brown et al., 2021). Changes in lake ice coverage, and hence, seasonality of the diatom bloom seem also unlikely processes as these would also change moderately in a deep basin such as Lake Bolshoye Shchuchye.

For a significant change in the isotope composition of a lake, another option is substitution of lake water, i.e. a certain volume being replaced by isotopically different water. In mountainous areas such as the Polar Urals, water of lighter isotope composition than the lake itself might be glacier or snow melt waters draining from higher altitudes into the lake (i. e. Meyer et al., 2015). Taking into account the recent $\delta^{18}O_{lake}$ of −15.8‰ and assuming the present-day volume as constant and 100%, it can be calculated, how much water needs to be exchanged in Lake Bolshoye Shchuchye to explain an isotopic difference $\Delta^{18}O$ of 5‰. If this isotopically different inflow would correspond to the lightest snow measured within the catchment (−25‰; Fig. 3C), corresponding to a ~10‰ offset compared to $\delta^{18}O_{lake}$, about 55% of the lake water (equal to 0.55 km^3) need to be exchanged. Assuming lower snow endmember values of −30‰ and −35‰, less water would need to be replaced, but still amounting to 35% and 26% of the lake volume, respectively.

Adding large amounts of water from a different than usual source (with different water isotope composition) or cutting off the major source for a certain period could, hence, substantially change the isotope composition of the lake. At Two-Yurts-Lake (Kamchatka), the diatom oxygen isotope composition generally follows summer insolation. However, in Neoglacial times, this trend is amplified due to the addition of isotopically light water from melting glaciers (Meyer et al., 2015), even though there is currently no glaciation in the catchment. The more glacial meltwaters reach the lake, the more negative the inflow $\delta^{18}O$ and, hence, $\delta^{18}O_{lake}$. Less meltwater would imply lower contribution of isotopically light influx. If Lake Bolshoye Shchuchye received large amounts of glacier meltwater, this should be notable both in the sediment and hydrological records.

5.4. Glacier fluctuations

Glacier fluctuations are poorly constrained in the Russian Arctic, including the Polar Urals (Kononov et al., 2005; Solomina et al., 2010, 2015; Haflidason et al., 2019). It is known though that the glaciers in the Urals display exceptional changes in local accumulation (and ablation) budgets (Mangerud et al., 2008). Westerlies, especially in the winter season, favor accumulation of snow on leeward sides of the mountains. This process, combined with snow avalanches, leads to extremely high local accumulation rates, which may be several times higher than local precipitation (Mangerud et al., 2008). Therefore, the situation on leeward sides of the Ural Mountains allows for short-term changes of the local accumulation and water balance, and hence, implies the possibility of contribution of light isotopic (winter and/or high altitude) precipitation to the lake.

Svendsen et al. (2019) performed a detailed assessment of the glacial and environmental changes in the Polar Urals including geomorphological description, exposure ages and lake sediment coring. In their study, they concluded on a larger glaciation in the region during stage MIS 4 and more restricted mountain glaciers in MIS 2 and MIS 3, but only small glaciers in shaded areas of the Polar Urals during MIS 1 that formed during Late Holocene cooling. For the Ural Mountains, an endmoraine and glacier advances during the LIA age have been described (Mangerud et al., 2008).

A possibility to test our hypothesis of glacial meltwaters triggering centennial-scale changes in $\delta^{18}O_{lake}$ is a comparison with northern hemispheric (or Eurasian) glacial fluctuations as summarised in Solomina et al. (2015). Here, the Russian Arctic is poorly constrained, but several glacial advances have been described in Neoglacial times, generally associated with regional cooling i.e. for Franz Josef Land with a prominent advance in the LIA (Lubinsky et al., 1999). However, regional compilations of dated glacier advances exist for the Alps (Ivy-Ochs et al., 2009), Scandinavia (Nesje, 2009) or semi-arid Asia (Dortch et al., 2013), summarised in Solomina et al. (2015).

There is a notable similarity to the Scandinavian reconstruction (Nesje, 2009) with described glacial advances at 0.2–0.7, 1.6, 2.3, 3.3, 4.4, 5.6 cal Ka BP, corresponding to prominent minima in the Bolshoye Shchuchye $\delta^{18}O_{diatom}$ record (Fig. 4), which would correspond to enhanced influx of glacial meltwaters, either due to more winter precipitation or meltwater entering the lake lowering $\delta^{18}O_{lake}$. Other prominent minima in the $\delta^{18}O_{diatom}$ record at 6.6–6.8 and 7.4–7.7 cal Ka BP are, however, not found in the Scandinavian reconstruction by Nesje (2009), but either in the Alps, in Norway (Matthews and Dresser, 2008) or in semi-arid Asia (Dortch et al., 2013).

The centennial-scale fluctuations in the $\delta^{18}O_{diatom}$ record are roughly contemporaneous with northern hemisphere glacier advances, described for other Eurasian regions. Therefore, maxima in the Bolshoye Shchuchye $\delta^{18}O_{diatom}$ record could hence be associated with either reduced meltwater or winter precipitation influx to the lake either due to lower precipitation amounts or less snow transported to the leeward side of the Ural Mountains.

High-resolution glacier mass balance studies in the Polar Urals provide (additional) evidence for short-term snow changes in the region, with a generally positive glacier mass balance in the LIA and a negative mass balance after 1850 CE (Kononov et al., 2005). LIA moraines have been described for several glaciers in the Polar Urals, including the Chernov and Obruchev glaciers (Mangerud et al., 2008). The second part of the 20th century shows a pronounced tendency towards glacier shrinkage, with solid precipitation in the region being generally lower than the ablation (Khromova et al., 2014, 2019).

5.5. Lake-internal parameters

In order to test whether the strong variability in the Holocene $\delta^{18}O_{diatom}$ record at Lake Bolshoye Shchuchye with their clear, short-term centennial-scale fluctuations is also reflected in the lakes' sedimentary record, we inter-compare diatom oxygen isotopes and lake-internal parameters from Lenz et al. (2021). These parameters (Fig. 4) supposedly react on fast and major changes in the catchment hydrology and include abiotic (clay content and Ti cps) as well as biotic proxies (TOC, biogenic opal contents and chironomids).

All these proxies display some internal variability throughout the Holocene, but do not reveal statistically significant relationships with the $\delta^{18}O_{diatom}$ record. During Early Holocene the observed high representation of lotic chironomids can be related to a scarce lacustrine fauna at this time. Lotic chironomids are brought by riverine influx, i.e. fed by water from snowmelt and enrich the

lake benthic communities. Decrease in the share of lotic taxa thereafter can be related to a better development of the lacustrine fauna under milder climatic conditions during Mid Holocene. At ~7.5–8.5 cal Ka BP, when $\delta^{18}O_{diatom}$ shows a maximum and the diatom oxygen isotope variability increases clearly, a major phase shift is obvious in all lake-internal proxies with absolute maxima in biogenic opal, TOC and chironomid-derived summer T_{air}, as well as absolute minima in Ti and clay values.

At 7.5 cal Ka BP, the lake-internal parameters show a slight decrease in biogenic opal and chironomid-based summer temperatures, a moderate increase in Ti cps, and rather constant values in clay and TOC contents. Biogenic opal as indicator of the lakes' diatom production and chironomid-derived T_{July} show similarities to the diatom oxygen isotope record such as common Mid Holocene maxima and Late Holocene minima. Meltwater events should lead to enhanced nutrient supply to the lake and, thus, a higher biogenic opal concentration in the core. Some minima, e. g. at 0.01, 1.7, 4.2, 6.0, 6.7 and 9.5 cal Ka BP in the $\delta^{18}O_{diatom}$ record roughly correspond to maxima in the biogenic opal concentration (Fig. 4). Some of these $\delta^{18}O_{diatom}$ minima are related to maxima (e. g. at 0.01, 6.0 cal Ka BP) in the total amount of lotic chironomids (Fig. 4).

Despite lower frequency variations of biogenic opal compared to $\delta^{18}O_{diatom}$ and the absence of a statistically significant relationship between both, the transport of nutrients by inflow processes (by meltwaters) to the lake seems to be reflected in $\delta^{18}O_{diatom}$. The only other biotic proxy displaying a few similar, although not well-expressed maxima (i. e. at ~8.0, 6.4 and 2.0 cal Ka BP) is the TOC record as proxy for organic matter deposition of Lake Bolshoye Shchuchye (Lenz et al., 2021).

A recent study by Cowling et al. (2021) deduced changes in the summer water balance and moisture sources during deglaciation and Early Holocene, using leaf wax hydrogen isotopes at Lake Bolshoye Shchuchye. However, a significant enrichment of $\delta^{2}H_{leaf\ wax}$ values between 10.5 and 10.0 cal Ka BP does not correspond to the changes in the $\delta^{18}O_{diatom}$ signal (Fig. 4). This inconsistency can be related to uncertainties in the age models and temporal resolution of the datasets. Moreover, leaf waxes are related to (soil) water uptake into terrestrial and aquatic plants and their interpretation is more complicated for deriving the lake water isotope composition.

If we attribute the $\delta^{18}O_{diatom}$ fluctuations to glacial advances, they should also be reflected in abiotic proxies such as clay content or Ti cps at Lake Bolshoye Shchuchye, which were interpreted as indicators for glacial meltwater input and catchment erosion, respectively (Lenz et al., 2021). Although there is a similarity between these abiotic parameters in the Holocene, they are neither reflecting a similar overall trend, nor similar short-term variations as found in the $\delta^{18}O_{diatom}$ record.

Consequently, the hydrological changes inferred from the diatom oxygen isotopes have no clear linkage to the abiotic changes in the lake sediments, or these lake-internal proxies are not sensitive enough to record them. Hence, neither changes in glacial meltwater fluxes nor erosion levels in the catchment (as inferred from Ti cps and clay contents) can explain the short-term $\delta^{18}O_{diatom}$ variability. This suggests that glaciers in the catchment, if present in the Holocene, were either too small or too distant from the lake to have a major influence on the sediment record. Hence, the only water source that can plausibly explain the short-term fluctuations in the record is a change in the snow and its meltwater supply in the catchment, independent from glacier-derived meltwater.

5.6. Snow as key driver for short-term $\delta^{18}O_{diatom}$ fluctuations

Topographical features in the Polar Urals include leeward accumulation caused by persistent westerly winds, snow avalanches and shadowing-effects from mountain ridges. These factors can lead to a substantial (5–6 times, in the period 1958–1978) increase of the mean winter mass balance as compared to local precipitation (Mangerud et al., 2008). Presently, enhanced snow accumulation is strongly favored at higher elevations, on leeward slopes and in depressions (Voloshina, 1988). We draw the following conclusions from regional glacier mass balance studies: (1) the hydrology of the Polar Urals is strongly dominated by snow; (2) redistribution of snow may lead to a much higher SWE than actual precipitation (3) shadowing effects protect cirque glaciers and nival niches.

Fig. 6 displays the geomorphological and snow characteristics of the Lake Bolshoye Shchuchye catchment. The DEM in Fig. 6A and the derived slopes angles in Fig. 6B reveal steeply (up to 65°) incised valleys and several small streams draining into the lake. Generally, the catchment extends to the northwest of the lake with a maximum and mean elevation of about 1200 and 500 m a.s.l., respectively.

For calculating the snow distribution of the Lake Bolshoye Shchuchye catchment we used the precipitation amount from snow profiles of the nearby Bolshaya Khadata catchment (Gokhman and Zhidkov, 1979). Redistribution of snow may lead to a surplus of snow (reaching up to 8.45 m in snow height corresponding 3.40 m of snow-water equivalent; Fig. 6 C and D) in some areas of the catchment, especially in the higher altitudes and in narrow valleys in the northern/northwestern part of the catchment (Fig. 6). This suggests that in colder years, perennial snow fields may develop in leeside positions, storing there a surplus of accumulated snow and allowing for increased snow melt contribution in warmer years.

These specific regional characteristics described above must necessarily have an impact on the lake hydrology, even though there are currently no glaciers in the Bolshoye Shchuchye catchment (Fig. 1B). As pointed out, a direct impact of glacier advances and retreat in the catchment in the Holocene is unlikely as abiotic indicators in the Holocene lake sediments do not suggest abrupt changes of sediment sources.

We therefore assume snow changes within the catchment to be the main driver of the catchment's hydrology and, thus, responsible for the short-term fluctuations in the $\delta^{18}O_{diatom}$ record. Due to shadowing effects, only part of this snow melts in summer and discharges into the lake. In phases of stronger winds and/or more precipitation, the Bolshoye Shchuchye catchment on the leeward side of the Polar Urals can receive excess snow amounts. While the exact mechanisms of how the snow and the snow melt affect the lake are yet to be identified, two dominating effects can be assumed: (1) more snow precipitation and redistribution directly lead to more snow in the catchment, and hence, possibly to a higher snow-derived and isotopically-depleted influx to the lake, (2) a local warming and/or reduced shadowing effect (Mangerud et al., 2008) may provide more snow melt to the lake, especially when the catchment is snow-saturated.

Enhanced snow influx hence directly impacts on the lake water isotopic composition when more melt waters from higher altitudes with lighter isotopic composition are drained to the lake. Conversely, centennial-scale maxima as observed in the Bolshoye Shchuchye diatom oxygen isotope record could be attributed to short-term interruptions of snow melt supply to the lake due to reduced influx from higher altitudes, and hence, lead to isotopically heavier $\delta^{18}O_{diatom}$ values. The quick rebounds towards isotopically lighter values may then reflect a return to the "normal" conditions prevailing before these excursions: large amounts of snow being redistributed from the windward side of the Polar Urals towards the leeward side (into the Bolshoye Shchuchye catchment). However, parts of the variability could also be explained by

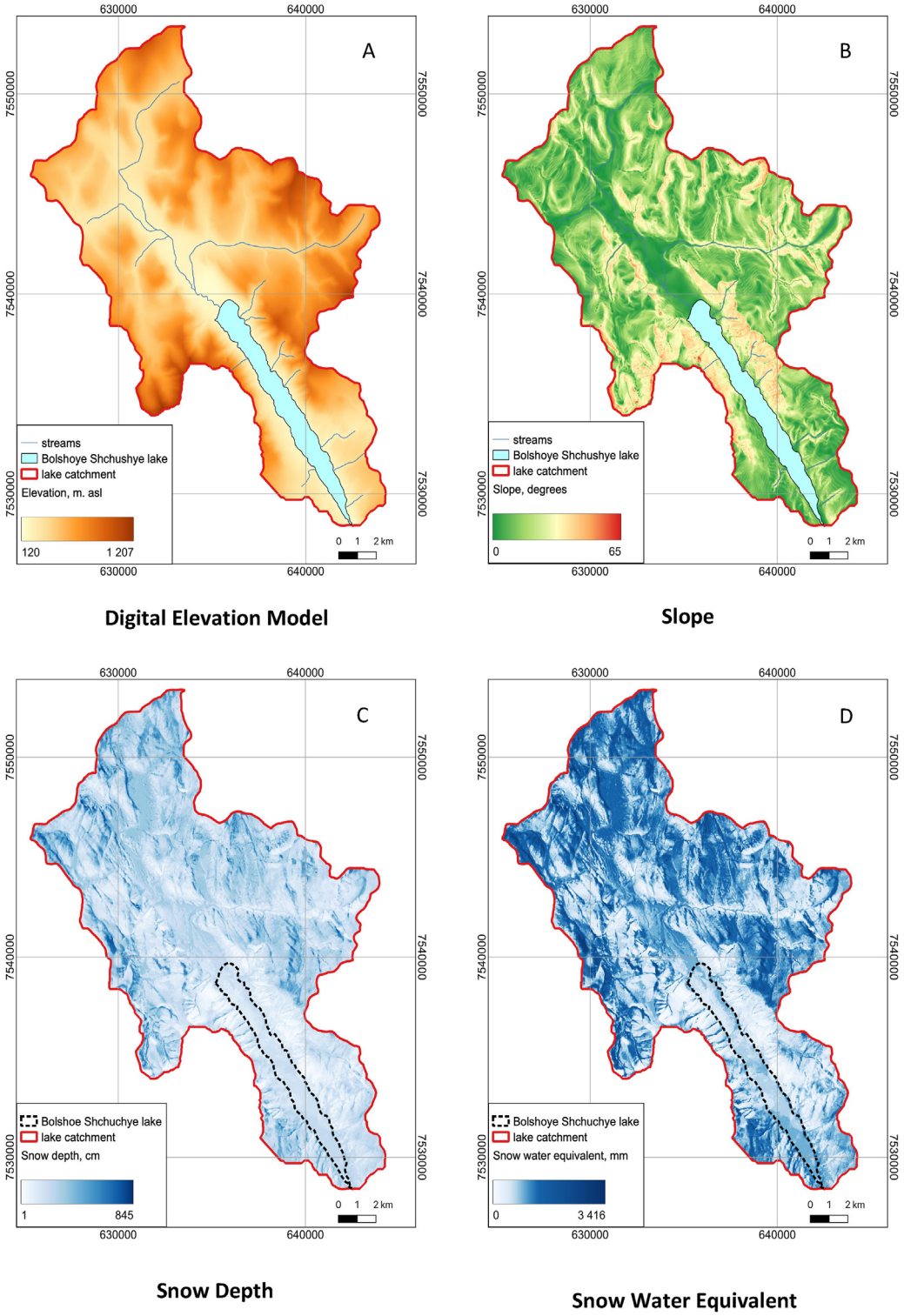

Fig. 6. Geomorphological and snow characteristics of the Lake Bolshoye Shchuchye catchment. (A) Digital Elevation Model (DEM), (B) Slope (in degrees), (C) snow depth (in cm) and (D) Snow water equivalent (SWE, in mm).

contributions of snow from different moisture sources (with a different isotope composition). This is also suggested by the missing reaction in local runoff and erosion proxies (Fig. 4), as it is likely that snowmelt is less effective at mobilizing sediments in the Bolshoye Shchuchye catchment than the glaciers during MIS 2 (Lenz et al., 2021; Haflidason et al., 2019).

In summary, the complex interplay between local hydroclimatic conditions with more snow delivered to the catchment (more P, stronger winds) and temporarily enhanced snow-melt phases (higher summer T) likely drives the observed short-term changes in the Bolshoye Shchuchye catchment. This mechanism allows for using the Bolshoye Shchuchye diatom oxygen isotopes as local

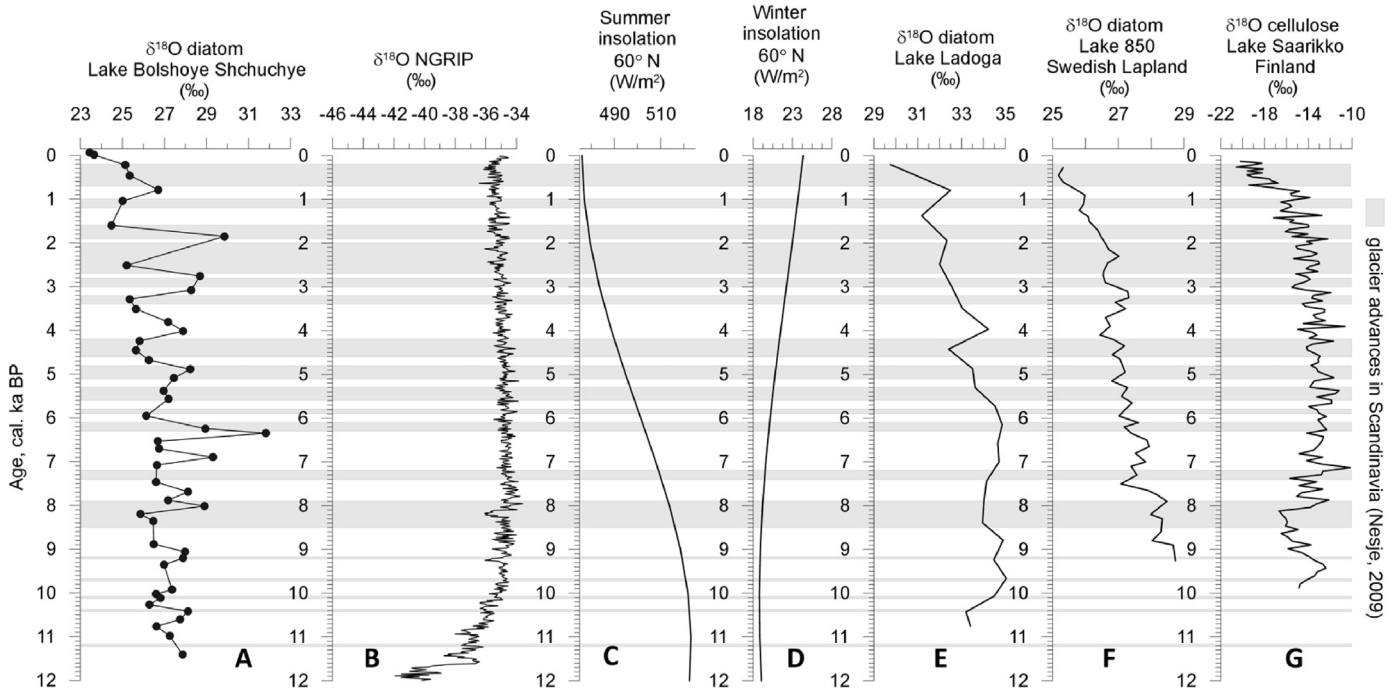

Fig. 7. (A) Oxygen isotope composition of diatoms from Lake Bolshoye Shchuchye compared to other North Hemispheric (NH) climate reconstructions, such as (B) the NGRIP oxygen isotope record from Greenland ice (Svensson et al., 2008), an proxy for the NH air temperature, (C and D) the NH summer and winter insolation at 60° N (Berger and Loutre, 1991), as well as other regional diatom-based oxygen isotope records (E) from Lake Ladoga (Kostrova et al., 2019) and (F) Lake 850, Swedish Lapland (Shemesh et al., 2001), and (G) a cellulose-based reconstruction from Lake Saariko, Finland (Heikkilä et al., 2010).

snow-melt indicator, hence as palaeo precipitation and summer temperature proxy.

6. Conclusions

Lake Bolshoye Shchuchye is a well-mixed lake, covered by ice for more than half of the year, with negligible evaporative effects, as derived from the recent water isotope dataset. The diatom oxygen isotope composition from the lacustrine sediments of Lake Bolshoye Shchuchye has been used as proxy for the hydrological and climate dynamics in the lake catchment.

During the Holocene, the Lake Bolshoye Shchuchye $\delta^{18}O_{diatom}$ record generally follows a decrease in summer insolation, in line with the northern hemisphere (NH) temperature history. However, Lake Bolshoye Shchuchye displays exceptional, short-term, centennial-scale changes exceeding 5‰, especially in Mid and Late Holocene roughly contemporaneous with NH glacier advances. As most of these minima and maxima are confirmed by more than one data point, these are considered not to be artefacts. Mixing calculations reveal that ~30–50% of the Lake Bolshoye Shchuchye water needs to be exchanged with isotopically different water within a short time to account for these shifts in $\delta^{18}O_{diatom}$. However, larger Holocene glacier advances in the Lake Bolshoye Shchuchye catchment are not known and have left no significant imprint on the lakes' abiotic proxies. Accordingly, a source of light isotope composition is snow, known to be transported in significant quantities, with large variability (and potentially relative contributions from different moisture sources) to the leeward side of the Polar Urals. Hence, we consider snow transport to the catchment and switch on/off of meltwater supply to the lake as the dominant hydrological process responsible for the observed short-term changes in the $\delta^{18}O_{diatom}$ record. A linkage between meltwater influx to lakes and $\delta^{18}O_{diatom}$ has been found before (Meyer et al., 2015). Here, however, centennial-scale hydrological changes have been documented in this high-latitude diatom oxygen isotope record, which, for this specific setting, are interpreted as indicator for palaeo precipitation, whereas the decreasing long-term trend in $\delta^{18}O_{diatom}$ follows summer temperature changes.

Author contribution

All authors have made substantial contributions to the manuscript: Hanno Meyer and Svetlana Kostrova designed and lead the study, analyzed and interpreted the diatom and water isotope datasets and wrote large parts of the manuscript. Philip Meister did the isotope hydrological model and its evaluation, whereas Marlene Lenz, Gerhard Kuhn brought in their sedimentological expertise and regional background (Lenz). Larisa Nazarova and Luidmila Syrtykh provided data, background and interpretation of chironomids as climate proxy. Yuri Dvornikov modelled the snow distribution and surface characteristics of the lake catchment. All authors have written parts of the manuscript, contributed to the interpretation and have approved its final version.

Declaration of competing interest

The authors declare that they have no known competing financial interests or personal relationships that could have appeared to influence the work reported in this paper.

Acknowledgements

The study was performed in the frame of the German-Russian projects 'PLOT – Paleolimnological Transect' (BMBF; grant 03G0859) and its successor 'PLOT – Synthesis' (BMBF; grant 03F0830C) both funded by the German Federal Ministry of Education and Research. We thank Ilona Schaepan from the German Research Center for Geosciences (GFZ) in Potsdam for the EDX

analyses, Rita Fröhlking-Teichert from the AWI Bremerhaven Marine Geology laboratory for BSi measurements, and Mikaela Weiner for technical support during sample preparation and isotope measurements at the AWI Potsdam stable isotope laboratory. Anna Ludikova from the Institute of Limnology, Russian Academy of Sciences, St. Petersburg is acknowledged for providing preliminary information on diatom taxonomy. Topographic and snow redistribution analyses were performed with support of the RUDN University Strategic Academic Leadership Program (Dr. Yuri Dvornikov). We thank the editor, Patrick Rioual, and three anonymous reviewers for their helpful and constructive comments.

Appendix A. Supplementary data

Supplementary data to this article can be found online at https://doi.org/10.1016/j.quascirev.2022.107620.

References

Andreev, A.A., Tarasov, P.E., Ilyashuk, B.P., Ilyashuk, E.A., Cremer, H., Hermichen, W.-D., Wischer, F., Hubberten, H.-W., 2005. Holocene environmental history recorded in lake Lyadhej-To sediments, Polar Urals, Russia. Palaeogeogr. Palaeoclimatol. Palaeoecol. 223, 181–203.

Astakhov, V.I., 2018. Late Quaternary glaciation of the northern Urals: a review and new observations. Boreas 47, 379–389.

Berger, A., Loutre, M.F., 1991. Insolation values for the climate of the last 10 million years. Quat. Sci. Rev. 10, 297–317.

Biskaborn, B.K., Nazarova, L., Pestryakova, L.A., Syrykh, L., Funck, K., Meyer, H., Chapligin, B., Vyse, S., Gorodnichev, R., Zakharov, E., Wang, R., Schwamborn, G., Diekmann, B., 2019. Spatial distribution of environmental indicators in surface sediments of Lake Bolshoe Toko, Yakutia, Russia. Biogeosciences 16 (20), 4023–4049. https://doi.org/10.5194/bg-2019-146.

Blaauw, M., 2010. Methods and code for 'classical' age-modelling of radiocarbon sequences. Quat. Geochronol. 5, 512–518.

Blaauw, M., 2021. Clam: Classical Age-Depth Modelling of Cores from Deposits. R package version 2.3.9.

Bogdanov, V.D., Bogdanova, E.N., Gavrilov, A.L., Melnichenko, I.P., Stepanov, L.N., Yarushina, M.I., 2004. Biological Resources of Aquatic Ecosystems of the Polar Urals. Publishing House of Ural Branch of RAS, Ekaterinburg, p. 168 in Russian.

Bonne, J.-L., Meyer, H., Behrens, M., Boike, J., Kipfstuhl, S., Rabe, B., Schmidt, T., Schönicke, L., Steen-Larsen, H.C., Werner, M., 2020. Moisture origin as a driver of temporal variabilities of the water vapour isotopic composition in the Lena River Delta, Siberia. Atmos. Chem. Phys. 20 (17), 10493–10511. https://doi.org/10.5194/acp-20-10493-2020.

Bowen, G.J., 2022. The Online Isotopes in Precipitation Calculator version OIPC3.1 (4/2017. http://www.waterisotopes.org.

Bowen, G.J., Revenaugh, J., 2003. Interpolating the isotopic composition of modern meteoric precipitation. Water Resour. Res. 39 (10), 1299, 10.129/2003WR002086.

Bowen, G.J., Wassenaar, L.I., Hobson, K.A., 2005. Global application of stable hydrogen and oxygen isotopes to wildlife forensics. Oecologia 143, 337–348.

Brooks, S.J., Langdon, P.G., Heiri, O., 2007. The identification and use of palaearctic chironomidae larvae in palaeoecology. In: QRA Technical Guide No. 10. Quaternary Research Association, London, p. 276.

Brown, S.R., Cartier, R., Schiller, C.M., Zahajská, P., Fritz, S.C., Morgan, L.A., Whitlock, C., Conley, D.J., Lacey, J.H., Leng, M.J., Shanks III, W.P., 2021. Multi-proxy record of Holocene paleoenvironmental conditions from Yellowstone Lake, Wyoming, USA. Quat. Sci. Rev. 274, 107275.

Cartier, R., Sylvestre, F., Paillès, C., Sonzogni, C., Couapel, M., Alexandre, A., Mazur, J.-C., Brisset, E., Miramont, C., Guiter, F., 2019. Diatom-oxygen isotope record from high-altitude Lake Petit (2200 m a.s.l.) in the Mediterranean Alps: shedding light on a climatic pulse at 4.2 ka. Clim. Past 15, 253–263.

Chapligin, B., Meyer, H., Friedrichsen, H., Marent, A., Sohns, E., Hubberten, H.-W., 2010. A high-performance, safer and semi-automated approach for the $\delta^{18}O$ analysis of diatom silica and new methods for removing exchangeable oxygen. Rapid Commun. Mass Spectrom. 24, 2655–2664.

Chapligin, B., Leng, M.J., Webb, E., Alexandre, A., Dodd, J.P., Ijiri, A., Lücke, A., Shemesh, A., Abelmann, A., Herzschuh, H., Longstaffe, F.J., Meyer, H., Moschen, R., Okazaki, Y., Rees, N.H., Sharp, Z.D., Sloane, H.J., Sonzongi, C., Swann, J.E.A., Sylvestre, F., Tyler, J.J., Yam, R., 2011. Inter-laboratory comparison of oxygen isotope compositions from biogenic silica. Geochem. Cosmochim. Acta 75, 7242–7256.

Chapligin, B., Meyer, H., Bryan, A., Snyder, J., Kemnitz, H., 2012a. Assessment of purification and contamination correction methods for analysing the oxygen isotope composition from biogenic silica. Chem. Geol. 300–301, 185–199.

Chapligin, B., Meyer, H., Swann, G.E.A., Meyer-Jacob, C., Hubberten, H.-W., 2012b. A 250-ka oxygen isotope record from diatoms at Lake El'gygytgyn, far east Russian Arctic. Clim. Past 8, 1621–1636. https://doi.org/10.5194/cp-8-1621-2012.

Clarke, C.L., Alsos, I.G., Edwards, M.E., Paus, A., Gielly, L., Haflidason, H., Mangerud, J., Regnéll, C., Hughes, P.D.M., Svendsen, J.I., Bjune, A.E., 2020. A 24,000-year ancient DNA and pollen record from the Polar Urals reveals temporal dynamics of arctic and boreal plant communities. Quat. Sci. Rev. 247, 106564.

Clayton, R., Mayeda, T., 1963. The use of bromine pentafluoride in the extraction of oxygen from oxides and silicates for isotopic analysis. Geochem. Cosmochim. Acta 27, 43–52.

Cowling, O., Thomas, E., Svendsen, J.I., Mangerud, J., Haflidason, H., Regnéll, C., Brendryen, J., 2021. The hydrologic cycle in western Siberia during the past 24,000 years changed in step with plant community structure. J. Quat. Sci. https://doi.org/10.1002/jqs.3386.

Craig, H., 1961. Isotopic variations in meteoric waters. Science 133, 1702–1703.

Cremer, H., Andreev, A., Hubberten, H.-W., Wischer, F., 2004. Paleolimnological reconstructions of Holocene environments and climate from lake lyadhej-to, ural mountains, northern Russia. Arctic Antarct. Alpine Res. 36, 147–155.

Dahl, S.O., Bakke, J., Lie, Ø., Nesje, A., 2003. Reconstruction of former glacier equilibrium-line altitudes based on proglacial sites: an evaluation of approaches and selection of sites. Quat. Sci. Rev. 22, 275–287.

Dansgaard, W., 1964. Stable isotopes in precipitation. Tellus 16 (4), 436–468.

Darling, W.G., Bath, A.H., Gibson, J.J., Rozanski, K., 2006. Isotopes in water. In: Leng, M.J. (Ed.), Isotopes in Paleoenvironmental Research, vol. 10. Springer, Dordrecht, pp. 1–52.

Davis, P.T., Menounos, B., Osborn, G., 2009. Holocene and latest Pleistocene alpine glacier fluctuations: a global perspective. Quat. Sci. Rev. 28, 2021–2033.

Dodd, J.P., Sharp, Z.D., 2010. A laser fluorination method for oxygen isotope analysis of biogenic silica and a new oxygen isotope calibration of modern diatoms in freshwater environments. Geochem. Cosmochim. Acta 74, 1381–1390.

Dortch, J.M., Owen, L.A., Caffee, M.W., 2013. Timing and climatic drivers for glaciation across semi-arid western Himalayan-Tibetan orogen. Quat. Sci. Rev. 78, 188–208.

Dushin, V.A., Serdyukova, O.P., Malyugin, A.A., Nikulina, I.A., Kozmin, V.S., Burmako, P.L., Abaturova, I.V., Kozmina, L.I., 2009. State geological map of the Russian federation 1:200000. In: Polar Ural Series. Sheet Q-42-I, II (Laborovaya). VSEGEI, St. Petersburg (in Russian).

Dvornikov, Y.A., Khomutov, A.V., Mullanurov, D.R., Ermokhina, K.A., Gubarkov, A.A., Leibman, M.O., 2015. GIS and field data based modelling of snow water equivalent in shrub tundra. Fennia 193 (1), 53–65. https://doi.org/10.11143/46363.

Evans, J.S., 2020. R spatialEco-Package (1.3-1). https://github.com/jeffreyevans/spatialEco.

Friedman, I., Benson, C., Cleason, J., 1991. Isotopic changes during snow metamorphism. In: Taylor, H.P., O'Neil, J.R., Kaplan, I.R. (Eds.), Stable Isotope Geochemistry: A Tribute to Samuel Epstein. The Geochemical Society. Special Publication No. 3, pp. 211–221.

Gardner, A.S., Moholdt, G., Cogley, J.G., Wouters, B., Arendt, A.A., Wahr, J., Berthier, E., Hock, R., et al., 2013. A reconciled estimate of glacier contributions to sea level rise: 2003 to 2009. Science 340, 852–857.

Gat, J.R., 1981. Lakes. In: Gat, J.R., Gonfiantini, R. (Eds.), Stable Isotope Hydrology - Deuterium and Oxygen-18 in the Water Cycle. IAEA, Vienna, pp. 203–221. Tech. Rep. Series No. 210.

Gibson, J.J., Edwards, T.W.D., Prowse, T.D., 1999. Pan-derived isotopic composition of atmospheric water vapour and its variability in northern Canada. J. Hydrol. 217, 55–74.

Gibson, C.E., Anderson, N.J., Haworth, E.Y., 2003. *Aulacoseira subarctica*: taxonomy, physiology, ecology and palaeoecology. Eur. J. Phycol. 38, 83–101.

Gokhman, V.V., Zhidkov, V.A., 1979. On the spatial distribution of snow storage in Polar Urals. In: Kotlyakov, V.M. (Ed.), Data of Glaciological Studies. Academy of Sciences USSR, pp. 177–182.

Gonfiantini, R., 1986. Environmental isotopes in lake studies. In: Fritz, O., Fontes, J.C. (Eds.), Handbook of Environmental Isotope Geochemistry: Vol 2, the Terrestrial Environment, B. Elsevier, Amsterdam, pp. 113–168.

Gorelick, N., Hancher, M., Dixon, M., Ilyushchenko, S., Thau, D., Moore, R., 2017. Google Earth engine: planetary-scale geospatial analysis for everyone. Remote Sens. Environ. 202, 18–27. https://doi.org/10.1016/J.RSE.2017.06.031.

Haflidason, H., Zweidorff, J.L., Baumer, M., Gyllencreutz, R., Svendsen, J.I., Gladysh, V., Logvina, E., 2019. The lastglacial and Holocene seismostratigraphy and sediment distribution of Lake Bolshoye Shchuchye, Polar Ural mountains, Arctic Russia. Boreas 48, 452–469.

Heikkilä, M., Edwards, T.W.D., Seppä, H., Sonninen, E., 2010. Sediment isotope tracers from Lake Saarikko, Finland, and implications for Holocene hydroclimatology. Quat. Sci. Rev. 29 (17–18), 2146–2160. https://doi.org/10.1016/j.quascirev.2010.05.010.

Huggel, C., Haeberli, W., Kääb, A., 2008. Glacial hazards: perceiving and responding to threats in four world regions. In: Orlove, B., Wiegandt, E., Luckman, B.H. (Eds.), Darkening Peaks. Glacier Retreat, Science and Society. University of California Press, Berkeley, US, pp. 68–80.

Hutchinson, M.F., 1989. A new procedure for gridding elevation and stream line data with automatic removal of spurious pits. J. Hydrol. 106, 211–232. https://doi.org/10.1016/0022-1694(89)90073-5.

IAEA/WMO, 2022. Global Network of isotopes in precipitation. In: The GNIP Database. https://nucleus.iaea.org/wiser.

IPCC, 2014. Climate Change 2014: Synthesis report. In: Core Writing Team, Pachauri, R.K., Meyer, L.A. (Eds.), Contribution of Working Groups I, II and III to the Fifth Assessment Report of the Intergovernmental Panel on Climate Change. IPCC, Geneva, pp. 1–151.

Ivanov, M.N., 2013. In: Lukashov, A.A., Troshkina, E.S. (Eds.), Evolution of Glaciation of the Polar Urals in the Late Holocene. Faculty of Geography, MSU.
Ivy-Ochs, S., Kerschner, H., Maisch, M., Christl, M., Kubik, P.W., Schluechter, C., 2009. Latest Pleistocene and Holocene glacier variations in the European Alps. Quat. Sci. Rev. 28, 2137–2149.
Jankovská, V., Andreev, A.A., Panova, N.K., 2006. Holocene environmental history on the eastern slope of the Polar Ural Mountains, Russia. Boreas 35, 650–661.
Jones, V.J., Leng, M.J., Solovieva, N., Sloane, H.J., Tarasov, P., 2004. Holocene climate of the Kola Peninsula; evidence from the oxygen isotope record of diatom silica. Quat. Sci. Rev. 23, 833–839.
Juggins, S., 2007. C2 Version 1.5 User Guide. Software for Ecological and Palaeoecological Data Analysis and Visualization. Newcastle University, Newcastle upon Tyne, UK.
Juillet-Leclerc, A., Labeyrie, L., 1987. Temperature dependence of the oxygen isotopic fractionation between diatom silica and water. Earth Planet Sci. Lett. 84, 69–74.
Kemmerich, A.O., 1966. The Polar Urals. Publishing House Fizkultura i Sport, Moscow, p. 112 (in Russian).
Khromova, T., Nosenko, G., Kutuzov, S., Muraviev, A., Chernova, L., 2014. Glacier area changes in Northern Eurasia. Environ. Res. Lett. 9, 015003.
Khromova, T., Nosenko, G., Nikitin, S., Muraviev, A., Popova, V., Chernova, L., Kidyaeva, V., 2019. Changes in the mountain glaciers of continental Russia during the twentieth to twenty-first centuries. Reg. Environ. Change 19, 1229–1247.
Koboltschnig, G.R., Schöner, W., 2011. The relevance of glacier melt in the water cycle of the Alps: the example of Austria. Hydrol. Earth Syst. Sci. 15, 2039–2048.
Kononov, Y.M., Ananicheva, M.D., Willis, I.C., 2005. High-resolution reconstruction of Polar Ural glacier mass balance for the last millennium. Ann. Glaciol. 42, 163–170.
Kostrova, S.S., Meyer, H., Chapligin, B., Kossler, A., Bezrukova, E.V., Tarasov, P.E., 2013. Holocene oxygen isotope record of diatoms from Lake Kotokel (southern Siberia, Russia) and its palaeoclimatic implications. Quat. Int. 290–291, 21–34.
Kostrova, S.S., Meyer, H., Chapligin, B., Tarasov, P.E., Bezrukova, E.V., 2014. The last glacial maximum and late glacial environmental and climate dynamics in the Baikal region inferred from an oxygen isotope record of lacustrine diatom silica. Quat. Int. 348, 25–36.
Kostrova, S.S., Meyer, H., Bailey, H.L., Ludikova, A.V., Gromig, R., Kuhn, G., Shibaev, Y.A., Kozachek, A.V., Ekaykin, A.A., Chapligin, B., 2019. Holocene hydrological variability of Lake Ladoga, northwest Russia, as inferred from diatom oxygen isotopes. Boreas 48, 361–376.
Kostrova, S.S., Biskaborn, B.K., Pestryakova, L.A., Fernandoy, F., Lenz, M.M., Meyer, H., 2021. Climate and environmental changes of the Lateglacial transition and Holocene in northeastern Siberia: evidence from diatom oxygen isotopes and assemblage composition at Lake Emanda. Quat. Sci. Rev. 259, 106905. https://doi.org/10.1016/j.quascirev.2021.106905.
Labeyrie, L.D., 1974. New approach to surface seawater palaeotemperatures using $^{18}O/^{16}O$ ratios in silica of diatom frustules. Nature 248, 40–42.
Lammers, Y., Clarke, C.L., Erséus, C., Brown, A.G., Edwards, M.E., Gielly, L., Haflidason, H., Mangerud, J., Rota, E., Svendsen, J.I., Alsos, I.G., 2019. Clitellate worms (Annelida) in lateglacial and Holocene sedimentary DNA records from the Polar Urals and northern Norway. Boreas 48, 317–329.
Lawrence, M., 2005. The relationship between relative humidity and the dewpoint temperature in moist air: a simple conversion and applications. Bull. Am. Meteorol. Soc. 86, 225–233.
Leng, M.J., Barker, P.A., 2006. A review of the oxygen isotope composition of lacustrine diatom silica for palaeoclimate reconstruction. Earth Sci. Rev. 75, 5–27.
Lenz, M.M., Andreev, A., Nazarova, L., Syrykh, L.S., Scheidt, S., Haflidason, H., Meyer, H., Brill, D., Wagner, B., Gromig, R.N., Lenz, M., Rolf, C., Kuhn, G., Fedorov, G., Svendsen, J.I., Melles, M., 2021. Climate and environmental history of the polar ural mountains since early MIS 2 inferred from a 54-m-long sediment core from lake Bolshoye Shchuchye. J. Quat. Sci. https://doi.org/10.1002/jqs.3400.
Lepskaya, E.V., Jewson, D.H., Usoltseva, M.V., 2010. *Aulacoseira subarctica* in Kurilskoye Lake, Kamchatka: a deep, oligotrophic lake and important pacific salmon nursery. Diatom Res. 25 (2), 323–335.
Linacre, E.T., 1977. A simple formula for estimating evaporation rates in various climates, using temperature data alone. Agric. Meteorol. 18, 409–424.
Lubinsky, D.J., Forman, S.L., Miller, G.H., 1999. Holocene glacier and climate fluctuations on Franz Josef Land, Arctic Russia, 80° N. Quat. Sci. Rev. 18 (1), 85–108.
Mangerud, J., Gosse, J., Matiouchkov, A., Dolvik, T., 2008. Glaciers in the Polar Urals, Russia, were not much larger during the last global glacial maximum than today. Quat. Sci. Rev. 27, 1047–1057.
Matthews, J.A., Dresser, P.Q., 2008. Holocene glacier variation chronology of the Smørstabbtinden massif, Jotunheimen, southern Norway, and the recognition of century- to millennial-scale European Neoglacial events. Holocene 18, 181–201.
Meyer, H., Schönicke, L., Wand, U., Hubberten, H.-W., Friedrichsen, H., 2000. Isotope studies of hydrogen and oxygen in ground ice – experiences with the equilibration technique. Isot. Environ. Health Stud. 36, 133–149.
Meyer, H., Chapligin, B., Hoff, U., Nazarova, L., Diekmann, B., 2015. Oxygen isotope composition of diatoms as late Holocene climate proxy at Two-Yurts Lake, central Kamchatka, Russia. Global Planet. Change 134, 118–128.
Mitrofanova, E.Y., 2017. Phytoplankton of the lake Bolshoe Shchuchye and rivers of its basin in August 2016. Scientific Newsletter of Yamalo-Nenets Autonomous Region 1 (94), 55–61 (in Russian).
Moller Pillot, H.K.M., 2009. Chironomidae Larvae. Biology and Ecology of the Chironomini. KNNV Publishing, Zeist, p. 270.
Moller Pillot, H.K.M., 2013. Chironomidae Larvae of the Netherlands and Adjacent Lowlands. In: Biology and Ecology of the Aquatic Orthocladiinae, vol. 3. KNNV Publishing, Zeist, Netherlands, p. 312.
Morozova, L.M., Magomedova, M.A., Ektova, S.N., Dyachenko, A.P., Knyazev, M.S. (Eds.), 2006. Vegetation Cover and Plant Resources of the Polar Urals. Publishing House of the Ural University, Yekaterinburg, p. 796 (in Russian).
Mortlock, R.D., Froelich, P.N., 1989. A simple method for the rapid determination of biogenic opal in pelagic marine sediments. Deep-Sea Res. 36, 1415–1426.
Müller, P.J., Schneider, R., 1993. An automated leaching method for the determination of opal in sediments and particulate matter. Deep Sea Res. Part I 40, 425–444.
Nazarova, L., Herzschuh, U., Wetterich, S., Kumke, T., Pestjakova, L., 2011. Chironomid-based inference models for estimating mean July air temperature and water depth from lakes in Yakutia, northeastern Russia. J. Paleolimnol. 45, 57–71.
Nazarova, L., Self, A., Brooks, S.J., van Hardenbroek, M., Herzschuh, U., Diekmann, B., 2015. Northern Russian chironomid-based modern summer temperature data set and inference models. Global Planet. Change 134, 10–25.
Nazarova, L., Bleibtreu, A., Hoff, U., Dirksen, V., Diekmann, B., 2017a. Changes in temperature and water depth of a small mountain lake during the past 3000 years in Central Kamchatka reflected by chironomid record. Quat. Int. 447, 46–58.
Nazarova, L.B., Self, A.E., Brooks, S.J., Solovieva, N., Syrykh, L.S., Dauvalter, V.A., 2017b. Chironomid fauna of the lakes from the pechora river basin (east of European part of Russian arctic): ecology and reconstruction of recent ecological changes in the region. Contempor. Probl. Ecol. 10, 350–362.
Nazarova, L., Grebennikova, T.A., Razjigaeva, N.G., Ganzey, L.A., Belyanina, N.I., Arslanov, K.A., Kaistrenko, V.M., Gorbunov, A.O., Kharlamov, A.A., Rudaya, N., Palagushkina, O., Biskaborn, B.K., Diekmann, B., 2017c. Reconstruction of Holocene environmental changes in southern kurils (North-Western pacific) based on palaeolake sediment proxies from shikotan island. Global Planet. Change 159, 25–36. https://doi.org/10.1016/j.gloplacha.2017.10.005.
Nazarova, L., Sachse, D., Fuchs, H.G.E., Dirksen, V., Dirksen, O., Syrykh, L., Razjigaeva, N.G., Diekmann, B., 2021a. Holocene evolution of a proglacial lake in southern Kamchatka, Russian Far East. Boreas. https://doi.org/10.1111/bor.12554.
Nazarova, L., Frolova, L.A., Palagushkina, O.V., Rudaya, N.A., Syrykh, L.S., Grekov, I.M., Solovieva, N., Loskutova, O.A., 2021b. Recent shift in biological communities: a case study from the Eastern European Russian Arctic (Bol'shezemelskaya Tundra). Polar Biol. https://doi.org/10.1007/s00300-021-02876-7.
Nesje, A., 2009. Latest Pleistocene and Holocene alpine glacier fluctuations in Scandinavia. Quat. Sci. Rev. 28, 2119–2136.
Nesje, A., Bakke, J., Brooks, S.J., Kaufman, D.S., Kihlberg, E., Trachsel, M., D'Andrea, W.J., Matthews, J.A., 2014. Late glacial and Holocene environmental changes inferred from sediments in Lake Myklevatnet, Nordfjord, western Norway. Veg. Hist. Archaeobotany 23, 229–248.
Nikolaev, V.I., Mikhalev, D.V., 1995. An oxygen-isotope paleothermometer from ice in Siberian permafrost. Quat. Res. 43, 14–21.
NOAA NCEI, 2020. NOAA National Centers for Environmental Information. State of the Climate: Global Climate Report for April 2020 published online May 2020, retrieved on May 26, 2020. https://www.ncdc.noaa.gov/sotc/global/202004.
Nosenko, G., Tsvetkov, D., 2003. Assessment of glaciers change on Polar Urals from ASTER imagery. In: Glaciological Data. Report GD-32. National Snow and Ice Data Center, Boulder, pp. 80–82.
Panova, N.K., Jankovska, V., Korona, O.M., Zinov'ev, E.V., 2003. The Holocene dynamics of vegetation and ecological conditions of the Polar Urals. Russ. J. Ecol. 34, 219–230.
Pechkin, A.S., Kirillov, V.V., Koveshnikov, M.I., Krasnenko, A.S., Saltykov, A.V., Timkin, A.V., Dyachenko, A.V., 2017. Morphometric characteristics of the lake bolshoe Shchuchye. Sci. Newsl. Yamalo-Nenets Autonom. Reg. 3 (96), 48–52 (in Russian).
Petrakov, D.A., Chernomorets, S.S., Evans, S.G., Tutubalina, O.V., 2008. Catastrophic glacial multi-phase mass movements: a special type of glacial hazard. Adv. Geosci. 14, 211–218.
Pischalnikova, E.V., 2016. Circulation conditions of abundant snowfalls formation in Perm region. Geogr. Bull. 1 (36), 70–77 (in Russian).
Porter, C., Morin, P., Howat, I., Noh, M.-J., Bates, B., Peterman, K., Keesey, S., Schlenk, M., Gardiner, J., Tomko, K., et al., 2018. *ArcticDEM*. Harvard Dataverse, V1. https://doi.org/10.7910/DVN/OHHUKH.
Quinn, P., Beven, K.J., Lamb, R., 1995. The in (a/tan/beta) index: how to calculate it and how to use it within the Topmodel framework. Hydrol. Process. 9 (2), 161–182.
R Core Team, 2017. R: A Language and Environment for Statistical Computing. R Foundation for Statistical Computing. https://www.r-project.org/.
R Core Team, 2020. R: A Language and Environment for Statistical Computing. R Foundation for Statistical Computing. https://www.r-project.org/.
Radić, V., Hock, R., 2014. Glaciers in the Earth's hydrological cycle: assessments of glacier mass and runoff changes on global and regional scales. Surv. Geophys. 35, 813–837.
Regnéll, C., Haflidason, H., Mangerud, J., Svendsen, J.I., 2019. Glacial and climate history of the last 24 000 years in the Polar Ural Mountains, Arctic Russia, inferred from partly varved lake sediments. Boreas 48, 432–443.
Robert, J.H., van Etten, J., 2012. R-Package Raster: Geographic Analysis and Modeling

with Raster Data (2.0-12). http://cran.r-project.org/package=raster.
Rozanski, K., Araguás-Araguás, L., Gonfiantini, R., 1993. Isotopic patterns in modern global precipitation. Geophysical Monograph 78. In: Climate Change in Continental Isotope Records. American Geophysical Union Monograph, pp. 1–36.
Shahgedanova, M., Nosenko, G., Bushueva, I., Ivanov, M., 2012. Changes in area and geodetic mass balance of small glaciers, Polar Urals, Russia, 1950–2008. J. Glaciol. 58 (211), 953–964.
Shemesh, A., Rosqvist, G., Rietti-Shati, M., Rubensdotter, L., Bigler, C., Yam, R., Karlen, W., 2001. Holocene climatic change in Swedish Lapland inferred from an oxygen-isotope record of lacustrine biogenic silica. Holocene 11 (4), 447–454.
Solomina, O., Ivanov, M., Bradwell, T., 2010. Lichenometric studies on moraines in the polar Urals. Geogr. Ann. Phys. Geogr. 92 (1), 81–99.
Solomina, O.N., Bradley, R.S., Hodgson, D.A., Ivy-Ochs, S., Jomelli, V., Mackintosh, A.N., Nesje, A., Owen, L.A., Wanner, H., Wiles, G.C., Young, N.E., 2015. Holocene glacier fluctuations. Quat. Sci. Rev. 111, 9–34.
Solovieva, N., Jones, V.J., Birks, H.J.B., Appleby, P.G., Nazarova, L., 2008. Diatom responses to 20th century climate warming in lakes from the northern Urals, Russia. Palaeogeogr. Palaeoclimatol. Palaeoecol. 259, 96–106.
Stief, P., Nazarova, L., De Beer, D., 2005. Chimney construction by *Chironomus riparius* larvae in response to hypoxia: microbial implications for freshwater sediments. J. North Am. Benthol. Soc. 24 (4), 858–871.
Svendsen, J.I., Alexanderson, H., Astakhov, V.I., Demidov, I., Dowdeswell, J.A., Funder, S., Gataullin, V., Henriksen, et al., 2004. Late Quaternary ice sheet history of northern Eurasia. Quat. Sci. Rev. 23 (11), 1229–1272. https://doi.org/10.1016/j.quascirev.2003.12.008.
Svendsen, J.I., Krüger, L.C., Mangerud, J., Astakhov, V.I., Paus, A., Nazarov, D., Murray, A., 2014. Glacial and vegetation history of the polar ural mountains in northern Russia during the last ice age, marine isotope stages 5–2. Quat. Sci. Rev. 92, 409–428.
Svendsen, J.I., Færseth, L.M.B., Gyllencreutz, R., Haflidason, H., Henriksen, M., Hovland, M.N., Lohne, Ø.S., Mangerud, J., et al., 2019. Glacial and environmental changes over the last 60 000 years in the Polar Ural Mountains, Arctic Russia, inferred from a high-resolution lake record and other observations from adjacent areas. Boreas 48, 407–431.
Svensson, A., Andersen, K.K., Bigler, M., Clausen, H.B., Dahl-Jensen, D., Davies, S.M., Johnsen, S.J., Muscheler, R., et al., 2008. A 60.000 year Greenland stratigraphic ice core chronology. Clim. Past 4, 47–57.
Swann, G.E.A., Leng, M.J., 2009. A review of diatom $\delta^{18}O$ in palaeoceanography. Quat. Sci. Rev. 28, 384–398.
Swann, G.E.A., Leng, M.J., Juschus, O., Melles, M., Brigham-Grette, J., Sloane, H.J., 2010. A combined oxygen and silicon diatom isotope record of Late Quaternary change in Lake El'gygytgyn, North East Siberia. Quat. Sci. Rev. 29, 774–786. https://doi.org/10.1016/j.quascirev.2009.11.024.
van Hardenbroek, M., Chakraborty, A., Davies, K.L., Harding, P., Heiri, O., Henderson, A.C.G., Holmes, J.A., Lasher, G.E., et al., 2018. The stable isotope composition of organic and inorganic fossils in lake sediment records: current understanding, challenges, and future directions. Quat. Sci. Rev. 196, 154–176.
Vinokurova, G.V., 2017. Phytoepilithon of the Lake Bolshoe Shchuchye and rivers flowing into and out of it (the Polar Urals). Sci. Newsl. Yamalo-Nenets Autonom. Reg. 1 (94), 11–14 (in Russian).
Voloshina, A., 1988. Some results of glacier mass balance research on the glaciers in the Polar Urals. Polar Geogr. Geol. 12, 200–211.
WGMS, 2017. In: Zemp, M., Nussbaumer, S.U., Gärtner-Roer, I., Huber, J., Machguth, H., Paul, F., Hoelzle, M. (Eds.), Global Glacier Change Bulletin No. 2 (2014–2015), ICSU(WDS)/IUGG(IACS)/UNEP/UNESCO/WMO. World Glacier Monitoring Service, Zurich, Switzerland, p. 244.
Wiederholm, T., 1983. Chironomidae of the holarctic region, keys and diagnoses. Part 1. Larvae: Entomol. Scand. Suppl. 19, 1–457.
Yermolaeva, N.I., Burmistrova, O.S., 2017. Zooplankton of the Lake Bolshoe Shchuchye. Sci. Newsl. Yamalo-Nenets Autonom. Reg. 1 (94), 15–20 (in Russian).